

1 Erosion of somatic tissue identity with loss of the X-linked
2 intellectual disability factor KDM5C

3

4 Katherine M. Bonefas^{1,2}, Ilakkia Venkatachalam^{2,3}, and Shigeki Iwase².

5 1. Neuroscience Graduate Program, University of Michigan Medical School, Ann Arbor, MI, 48109, USA.

6 2. Department of Human Genetics, Michigan Medicine, University of Michigan Medical School, Ann Arbor,
7 MI, 48109, USA.

8 3. Genetics and Genomics Graduate Program, University of Michigan, Ann Arbor, MI, 48109, USA.

9 Abstract

10 Mutations in numerous chromatin-modifying enzymes cause neurodevelopmental disorders (NDDs)
11 with unknown mechanisms. Loss of repressive chromatin regulators can lead to the aberrant transcription
12 of tissue-specific genes outside of their intended context, however the mechanisms and consequences
13 of their dysregulation are largely unknown. Here, we examine how lysine demethylase 5c (KDM5C), an
14 eraser of histone 3 lysine 4 di and tri-methylation (H3K4me2/3) that is mutated in Claes-Jensen X-linked
15 intellectual disability, contributes to tissue identity. We found male *Kdm5c* knockout (-KO) mice, which
16 recapitulate key human neurological phenotypes, aberrantly expresses many liver, muscle, ovary, and testis
17 genes within the amygdala and hippocampus. Gonad-enriched genes misexpressed in the *Kdm5c*-KO
18 brain are unique to germ cells, indicating an erosion of the soma-germline boundary. Germline genes are
19 typically decommissioned in somatic lineages in the post-implantation epiblast, yet *Kdm5c*-KO epiblast-like
20 cells (EpiLCs) aberrantly expressed key regulators of germline identity and meiosis, including *Dazl* and
21 *Stra8*. Characterizing germline gene misexpression in males and female mutants revealed germline gene
22 repression is sexually dimorphic, with female EpiLCs requiring a higher dose of KDM5C to maintain germline
23 gene suppression. Using a comprehensive list of mouse germline-enriched genes, we found KDM5C is
24 selectively recruited to a subset of germline gene promoters that contain CpG islands (CGIs) to facilitate
25 DNA CpG methylation (CpGme) during ESC to EpiLC differentiation. However, late stage spermatogenesis
26 genes devoid of promoter CGIs can also become activated in *Kdm5c*-KO cells via ectopic activation by RFX
27 transcription factors. Together, these data demonstrate KDM5C's fundamental role in tissue identity and
28 indicate that KDM5C acts as a break against runaway activation of germline developmental programs in
29 somatic lineages.

30 Introduction

31 A single genome holds the instructions to generate the myriad of cell types found within an organism.
32 This is, in part, accomplished by chromatin regulators that can either promote or impede lineage-specific
33 gene expression through DNA and histone modifications^{1–5}. Human genetic studies revealed mutations in
34 chromatin regulators are a major cause of neurodevelopmental disorders (NDDs)⁶ and many studies have
35 identified their importance for regulating brain-specific transcriptional programs. Loss of chromatin regulators
36 can also result in the ectopic expression of tissue-specific genes outside of their target environment, such
37 as the misexpression of liver-specific genes within adult neurons⁷. However, the mechanisms underlying
38 ectopic gene expression and its impact upon neurodevelopment are poorly understood.

39 To elucidate the role of tissue identity in chromatin-linked NDDs, it is essential to first characterize the
40 nature of the dysregulated genes and the molecular mechanisms governing their de-repression. Here we
41 focus on lysine demethylase 5C (KDM5C, also known as SMCX or JARID1C), which erases histone 3 lysine
42 4 di- and trimethylation (H3K4me2/3), a permissive chromatin modification enriched at gene promoters⁸.
43 Pathogenic mutations in the X chromosome gene *KDM5C* cause Intellectual Developmental Disorder, X-
44 linked, Syndromic, Claes-Jensen Type (MRXSCJ, OMIM: 300534). MRXSCJ is more common and severe
45 in males and its neurological phenotypes include intellectual disability, seizures, aberrant aggression, and
46 autistic behaviors^{9–11}. Male *Kdm5c* knockout (-KO) mice recapitulate key MRXSCJ phenotypes, including
47 hyperaggression, increased seizure propensity, social deficits, and learning impairments^{12–14}. RNA sequenc-
48 ing (RNA-seq) of the *Kdm5c*-KO hippocampus revealed ectopic expression of some germline genes within
49 the brain¹³. However, it is unclear if other tissue-specific genes are aberrantly transcribed with KDM5C loss,
50 at what point in development germline gene misexpression begins, and what mechanisms underlie their
51 dysregulation.

52 Distinguishing between germ cells and somatic cells is a key feature of multicellularity¹⁵ that occurs
53 during early embryogenesis in many metazoans¹⁶. In mammals, chromatin regulators are crucial for
54 decommissioning germline genes during the transition from naïve to primed pluripotency. Initially, germline
55 gene promoters gain repressive histone H2A lysine 119 monoubiquitination (H2AK119ub1)¹⁷ and histone
56 H3 lysine 9 trimethylation (H3K9me3)^{17,18} in embryonic stem cells (ESCs) and are then decorated with
57 DNA CpG methylation (CpGme) in post-implantation epiblast cells^{18–21}. The contribution of KDM5C to this
58 process remains unclear. Additionally, studies on germline gene repression have primarily been conducted
59 in males and focused on select marker genes important for early germ cell development, given the lack of a
60 comprehensive list for germline-enriched genes. Therefore, it is unknown if the mechanism of repression
61 differs between sexes or for different classes of germline genes, e.g. meiotic versus spermatid differentiation
62 genes.

63 To illuminate KDM5C's role in tissue identity, here we characterized the aberrant expression of tissue-
64 enriched genes within the *Kdm5c*-KO brain and epiblast-like stem cells (EpiLCs), an *in vitro* model of the

65 post-implantation embryo. We curated a list of mouse germline-enriched genes, which enabled genome-wide
66 analysis of germline gene silencing mechanisms for the first time. To illuminate the impact of sex upon
67 germline gene suppression, we characterized germline transcripts expressed in male and female *Kdm5c*
68 mutants. Based on the data presented below, we propose KDM5C plays a fundamental, sexually dimorphic
69 role in the development of tissue identity during early embryogenesis, including the establishment of the
70 soma-germline boundary.

71 Results

72 Tissue-enriched genes are aberrantly expressed in the *Kdm5c*-KO brain

73 Previous RNA sequencing (RNA-seq) of the adult male *Kdm5c*-KO hippocampus revealed ectopic
74 expression of some germline genes unique to the testis¹³. It is currently unknown if the testis is the only
75 tissue type misexpressed in the *Kdm5c*-KO brain. We thus systematically tested whether other tissue-specific
76 genes are misexpressed in the male brain with constitutive knockout of *Kdm5c* (*Kdm5c*^{-/-}, 5CKO)²² by using
77 a published list of mouse tissue-enriched genes²³.

78 We found a large proportion of significantly upregulated genes (DESeq2²⁴, log2 fold change > 0.5,
79 q < 0.1) within the male *Kdm5c*-KO amygdala and hippocampus are non-brain, tissue-specific genes
80 (Amygdala: 21/59 up DEGs, 35.59% ; Hippocampus: 51/183 up DEGs, 27.87%) (Figure 1A-B). For both the
81 amygdala and hippocampus, the majority of tissue-enriched differentially expressed genes (DEGs) were
82 testis genes (Figure 1A-B). Even though the testis has the largest total number of tissue-biased genes (2,496
83 genes) compared to any other tissue, testis-biased DEGs were significantly enriched for both brain regions
84 (Amygdala p = 1.83e-05, Odds Ratio = 5.13; Hippocampus p = 4.26e-11, Odds Ratio = 4.45, Fisher's Exact
85 Test). An example of a testis-enriched gene misexpressed in the *Kdm5c*-KO brain is *FK506 binding protein 6*
86 (*Fkbp6*), a known regulator of PIWI-interacting RNAs (piRNAs) and meiosis^{25,26} (Figure 1C).

87 Interestingly, we also observed significant enrichment of ovary-biased genes in both the amygdala and
88 hippocampus (Amygdala p = 0.00574, Odds Ratio = 18.7; Hippocampus p = 0.048, Odds Ratio = 5.88,
89 Fisher's Exact) (Figure 1A-B). Ovary-enriched DEGs included *Zygotic arrest 1* (*Zar1*), which sequesters
90 mRNAs in oocytes for meiotic maturation²⁷ (Figure 1D). Given that the *Kdm5c*-KO mice we analyzed are
91 male, these data demonstrate that the ectopic expression of gonad-enriched genes is independent of
92 organismal sex.

93 Although not consistent across brain regions, we also found significant enrichment of genes biased
94 towards two non-gonadal tissues - the liver (Amygdala p = 0.04, Odds Ratio = 6.58, Fisher's Exact Test) and
95 muscles (Hippocampus p = 0.01, Odds Ratio = 6.95, Fisher's Exact Test) (Figure 1A-B). *Apolipoprotein C-I*
96 (*Apoc1*) a lipoprotein metabolism and transport gene, is among the liver-biased DEG derepressed in both
97 the hippocampus and amygdala²⁸ and its brain overexpression has been implicated in Alzheimer's disease²⁹

98 (Figure 1E).

99 Analysis of oligo(dT)-primed libraries²² demonstrates aberrantly expressed mRNAs are polyadenylated
100 and spliced into mature transcripts in the *Kdm5c*-KO brain (Figure 1C-E). Of note, we observed little to no
101 dysregulation of brain-enriched genes (Amygdala p = 1, Odds Ratio = 1.22; Hippocampus p = 0.74, Odds
102 Ratio = 1.22, Fisher's Exact), despite the fact these are brain samples and the brain has the second highest
103 total number of tissue-enriched genes (708 genes). Altogether, these results suggest the aberrant expression
104 of tissue-enriched genes within the brain is a major effect of KDM5C loss.

105 **Germline genes are misexpressed in the *Kdm5c*-KO brain**

106 *Kdm5c*-KO brain expresses testicular germline genes¹³, however the testis also contains somatic cells that
107 support hormone production and germline functions. To determine if *Kdm5c*-KO results in ectopic expression
108 of somatic testicular genes, we first evaluated the known functions of testicular DEGs through gene ontology.
109 We found *Kdm5c*-KO testis-enriched DEGs had high enrichment of germline-relevant ontologies, including
110 spermatid development (GO: 0007286, p.adjust = 6.2e-12) and sperm axoneme assembly (GO: 0007288,
111 p.adjust = 2.45e-14) (Figure 2A).

112 We then evaluated testicular DEG expression in wild-type testes versus testes with germ cell depletion³⁰,
113 which was accomplished by heterozygous *W* and *Wv* mutations in the enzymatic domain of *c-Kit* (*Kit*^{W/Wv})³¹.
114 Almost all *Kdm5c*-KO testis-enriched DEGs lost expression with germ cell depletion (Figure 2B). We then
115 assessed testis-enriched DEG expression in a published single cell RNA-seq dataset that identified cell
116 type-specific markers within the testis³². Some *Kdm5c*-KO testis-enriched DEGs were classified as specific
117 markers for different germ cell developmental stages (e.g. spermatogonia, spermatocytes, round spermatids,
118 and elongating spermatids), yet none marked somatic cells (Figure 2C). Together, these data demonstrate
119 that the *Kdm5c*-KO brain aberrantly expresses germline genes but not somatic testicular genes, reflecting an
120 erosion of the soma-germline boundary.

121 As of yet, research on germline gene silencing mechanisms has focused on a handful of key genes rather
122 than assessing germline gene suppression genome-wide, due to the lack of a comprehensive gene list.
123 We therefore generated a list of mouse germline-enriched genes using RNA-seq datasets of *Kit*^{W/Wv} mice
124 that included males and females at embryonic day 12, 14, and 16³³ and adult male testes³⁰. We defined
125 genes as germline-enriched if their expression met the following criteria: 1) their expression is greater than
126 1 FPKM in wild-type gonads 2) their expression in any non-gonadal tissue of adult wild type mice²³ does
127 not exceed 20% of their maximum expression in the wild-type germline, and 3) their expression in the germ
128 cell-depleted gonads, for any sex or time point, does not exceed 20% of their maximum expression in the
129 wild-type germline. These criteria yielded 1,288 germline-enriched genes (Figure 2D), which was hereafter
130 used as a resource to globally characterize germline gene misexpression with *Kdm5c* loss (Supplementary
131 table 1).

132 ***Kdm5c*-KO epiblast-like cells aberrantly express key regulators of germline identity**

133 Germ cells are typically distinguished from somatic cells soon after the embryo implants into the uterine
134 wall^{34,35}, when germline genes are silenced in epiblast stem cells that will form the somatic tissues³⁶. This
135 developmental time point can be modeled *in vitro* through differentiation of naïve embryonic stem cells
136 (nESCs) into epiblast-like stem cells (EpiLCs) (Figure 3A)^{37,38}. While some germline-enriched genes are
137 also expressed in nESCs and in the 2-cell stage^{39–41}, they are silenced as they differentiate into EpiLCs^{18,19}.
138 Therefore, we tested if KDM5C was necessary for the initial silencing of germline genes in somatic lineages
139 by evaluating the impact of *Kdm5c* loss in male EpiLCs.

140 *Kdm5c*-KO cell morphology during ESC to EpiLC differentiation appeared normal (Figure 3B) and EpiLCs
141 properly expressed markers of primed pluripotency, such as *Dnmt3b*, *Fgf5*, *Pou3f1*, and *Otx2* (Figure 3C). We
142 then identified tissue-enriched DEGs in a RNA-seq dataset of wild-type and *Kdm5c*-KO EpiLCs⁴² (DESeq2,
143 log₂ fold change > 0.5, q < 0.1). Similar to the *Kdm5c*-KO brain, we observed general dysregulation of
144 tissue-enriched genes, with the largest number of genes belonging to the brain and testis, although they
145 were not significantly enriched (Figure 3D). Using our list of mouse germline-enriched genes assembled
146 above, we identified 68 germline genes misexpressed in male *Kdm5c*-KO EpiLCs.

147 We then compared EpiLC germline DEGs to those expressed in the *Kdm5c*-KO brain to determine if
148 germline genes are constitutively dysregulated or change over the course of development. The majority of
149 germline DEGs were unique to either EpiLCs or the brain, with only *D1Pas1* and *Cyct* shared across all
150 tissue/cell types (Figure 3E-F). EpiLC germline DEGs had particularly high enrichment of meiosis-related
151 gene ontologies when compared to the brain (Figure 3G), such as meiotic cell cycle process (GO:1903046,
152 p.adjust = 2.2e-07) and meiotic nuclear division (GO:0140013, p.adjust = 1.37e-07). While there was
153 modest enrichment of meiotic gene ontologies in both brain regions, the *Kdm5c*-KO hippocampus primarily
154 expressed late-stage spermatogenesis genes involved in sperm axoneme assembly (GO:0007288, p.adjust
155 = 0.00621) and sperm motility (GO:0097722, p.adjust = 0.00612).

156 Notably, DEGs unique to *Kdm5c*-KO EpiLCs included key drivers of germline identity, such as *Stimulated*
157 *by retinoic acid 8* (*Stra8*: log₂ fold change = 3.73, q = 2.17e-39) and *Deleted in azoospermia like* (*Dazl*: log₂
158 fold change = 3.36, q = 3.19e-12) (Figure 3H). These genes are typically expressed when primordial germ
159 cells (PGCs) are committed to the germline fate and again later in life to trigger meiotic gene expression
160 programs^{43–45}. Of note, some germline genes, including *Dazl*, are also expressed in the two-cell embryo^{40,46}.
161 However, we did not see derepression of two-cell stage-specific genes, like *Duxf3* (*Dux*) (log₂ fold change
162 = -0.282, q = 0.337) and *Zscan4d* (log₂ fold change = 0.25, q = 0.381) (Figure 3H), indicating *Kdm5c*-KO
163 EpiLCs do not revert back to a 2-cell state. Altogether, *Kdm5c*-KO EpiLCs express key drivers of germline
164 identity and meiosis while the brain primarily expresses spermiogenesis genes, indicating germline gene
165 misexpression mirrors germline development during the progression of somatic development.

166 **Female epiblast-like cells have increased sensitivity to germline gene misexpression**
167 **with *Kdm5c* loss**

168 It is currently unknown if the misexpression of germline genes is influenced by sex, as previous studies
169 on germline gene repressors have focused on male cells^{17,18,20,47,48}. Sex is particularly pertinent in the case
170 of KDM5C because it partially escapes X chromosome inactivation (XCI), resulting in a higher dosage in
171 females^{49–52}. We therefore explored the impact of chromosomal sex upon germline gene suppression by
172 comparing their dysregulation in male *Kdm5c* hemizygous knockout (XY *Kdm5c*-KO, XY 5CKO), female
173 homozygous knockout (XX *Kdm5c*-KO, XX 5CKO), and female heterozygous knockout (XX *Kdm5c*-HET, XX
174 5CHET) EpiLCs⁴².

175 In EpiLCs, homozygous and heterozygous *Kdm5c* knockout females expressed over double the number
176 of germline-enriched genes than hemizygous males (Figure 4A). While the majority of germline DEGs in
177 *Kdm5c*-KO males were also dysregulated in females (74%), many were sex-specific, such as *Tktl2* and *Esx1*
178 (Figure 4B). We then compared the known functions of germline genes dysregulated only in females, only in
179 males, or in all samples (Figure 4C). Female-specific germline DEGs were enriched for meiotic (GO:0051321
180 - meiotic cell cycle) and flagellar (GO:0003341 - cilium movement) functions, while male-specific DEGs had
181 roles in mitochondrial and cell signaling (GO:0070585 - protein localization to mitochondrion). Germline
182 transcripts expressed in both sexes were enriched for meiotic (GO:0140013 - meiotic nuclear division) and
183 egg-specific functions (GO:0007292 - female gamete generation).

184 The majority of germline genes expressed in both sexes were more highly dysregulated in females
185 compared to males (Figure 4D-F). This increased degree of dysregulation in females, along with the
186 increased total number of germline genes, indicates females are more sensitive to losing KDM5C-mediated
187 germline gene suppression. Heightened germline gene dysregulation in females could be due to impaired
188 XCI in *Kdm5c* mutants⁴², as many spermatogenesis genes lie on the X chromosome^{53,54}. However, female
189 germline DEGs were not biased towards the X chromosome and females had a similar overall proportion
190 of germline DEGs belonging to the X chromosome as males (XY *Kdm5c*-KO - 10.29%, XX *Kdm5c*-HET -
191 7.43%, XX *Kdm5c*-KO - 10.59%) (Figure 4G). The majority of germline DEGs instead lie on autosomes for
192 both male and female *Kdm5c* mutants (Figure 4G). Thus, while female EpiLCs are more prone to germline
193 gene misexpression with KDM5C loss, it is likely independent of XCI defects.

194 **Germline gene misexpression in *Kdm5c* mutants is independent of germ cell sex**

195 Although many germline genes have shared functions in the male and female germline, e.g. PGC
196 formation, meiosis, and genome defense, some have unique or sex-biased expression. Therefore, we
197 wondered if *Kdm5c* mutant males would primarily express sperm genes while mutant females would primarily
198 express egg genes. To comprehensively assess whether germline gene sex corresponds with *Kdm5c* mutant
199 sex, we first filtered our list of germline-enriched genes for egg and sperm-biased genes (Figure 4H). We

200 defined germ cell sex-biased genes as those whose expression in the opposite sex, at any time point, is
201 no greater than 20% of the gene's maximum expression in a given sex. This criteria yielded 0 egg-biased,
202 0 sperm-biased, and 197 unbiased germline-enriched genes. We found regardless of sex, egg, sperm,
203 and unbiased germline genes were dysregulated in all *Kdm5c* mutants at similar proportions (Figure 4I-J).
204 Furthermore, germline genes dysregulated exclusively in either male or female mutants were also not biased
205 towards their corresponding germ cell sex (Figure 4I). Altogether, these results demonstrate sex differences
206 in germline gene dysregulation is not due to sex-specific activation of sperm or egg transcriptional programs.

207 **KDM5C binds to a subset of germline gene promoters during early embryogenesis**

208 KDM5C binds to the promoters of several germline genes in embryonic stem cells (ESCs) but not in
209 neurons^{13,55}. However, the lack of a comprehensive list of germline-enriched genes prohibited genome-wide
210 characterization of KDM5C binding at germline gene promoters. Thus, it is unclear if KDM5C is enriched at
211 germline gene promoters, what types of germline genes KDM5C regulates, and if its binding is maintained at
212 any germline genes in neurons.

213 To address these questions, we analyzed KDM5C chromatin immunoprecipitation followed by DNA
214 sequencing (ChIP-seq) datasets in EpiLCs⁴² and primary forebrain neuron cultures (PNCs)¹² (MACS2 q
215 < 0.1, fold enrichment > 1, and removal of false-positive peaks in *Kdm5c*-KO). EpiLCs had a higher total
216 number of high-confidence KDM5C peaks than PNCs (EpiLCs: 5,808, PNCs: 1,276). KDM5C was primarily
217 localized to gene promoters in both cell types (promoters = transcription start site (TSS) ± 500 bp, EpiLCs:
218 4,190, PNCs: 745), although PNCs showed increased localization to non-promoter regions (Figure 5A).

219 The majority of promoters bound by KDM5C in PNCs were also bound in EpiLCs (513 shared promoters),
220 however a large portion of gene promoters were bound by KDM5C only in EpiLCs (3,677 EpiLC only
221 promoters) (Figure 5B). Genes bound by KDM5C in both PNCs and EpiLCs were enriched for functions
222 involving nucleic acid turnover, such as deoxyribonucleotide metabolic process (GO:0009262, p.adjust =
223 8.28e-05) (Figure 5C). Germline ontologies were enriched only in EpiLC-specific, KDM5C-bound promoters,
224 such as meiotic nuclear division (GO: 0007127 p.adjust = 6.77e-16) (Figure 5C). There were no significant
225 ontologies for PNC-specific KDM5C target genes. Using our mouse germline gene list, we observed evident
226 KDM5C signal around the TSS of many germline genes in EpiLCs, but not in PNCs (Figure 5D). Based
227 on our ChIP-seq peak cut-off criteria, KDM5C was highly enriched at 211 germline gene promoters in
228 EpiLCs (16.4% of all germline genes) (Figure 5E). Of note, KDM5C was only bound to about one third
229 of RNA-seq DEG promoters unique to EpiLCs or the brain (EpiLC only DEGs: 34.9%, Brain only DEGs:
230 30%) (Supplementary figure 1A-C). Representative examples of EpiLC DEGs bound and unbound by
231 KDM5C in EpiLCs are *Dazl* and *Stra8*, respectively (Figure 5F). However, the four of the five germline genes
232 dysregulated in both EpiLCs and the brain were bound by KDM5C in EpiLCs (*D1Pas1*, *Hsf2bp*, *Cyct*, and
233 *Stk31*) (Supplementary figure 1A). Together, these results demonstrate KDM5C is recruited to a subset
234 of germline genes in EpiLCs, including meiotic genes, but does not directly regulate germline genes in

235 neurons. Furthermore, the majority of germline mRNAs expressed in *Kdm5c*-KO cells are dysregulated
236 independent of direct KDM5C recruitment to their gene promoters, however genes dysregulated across
237 *Kdm5c*-KO development are often direct KDM5C targets.

238 Many germline-specific genes are suppressed by the polycomb repressive complex 1.6 (PRC1.6), which
239 contains transcription factor heterodimers E2F6/DP1 and MGA/MAX that respectively bind E2F and E-box
240 motifs⁵⁸. PRC1.6 members may recruit KDM5C to germline gene promoters¹³, given their association
241 with KDM5C in HeLa cells and ESCs^{46,59}. We thus used HOMER⁶⁰ to identify transcription factor motifs
242 enriched at KDM5C-bound or unbound germline gene promoters (TSS ± 500 bp, q-value < 0.1). MAX
243 and E2F6 binding sites were significantly enriched at germline genes bound by KDM5C in EpiLCs (MAX
244 q-value: 0.0068, E2F6 q-value: 0.0673, E2F q-value: 0.0917), but not at germline genes unbound by
245 KDM5C (Figure 5G). One third of KDM5C-bound promoters contained the consensus sequence for either
246 E2F6 (E2F, 5'-TCCCGC-3'), MGA (E-box, 5'-CACGTG-3'), or both, but only 17% of KDM5C-unbound genes
247 contained these motifs (Figure 5H). KDM5C-unbound germline genes were instead enriched for multiple
248 RFX transcription factor binding sites (RFX q-value < 0.0001, RFX2 q-value < 0.0001, RFX5 q-value <
249 0.0001) (Figure 5I, Supplementary figure 1D). RFX transcription factors bind X-box motifs⁶¹ to promote
250 ciliogenesis^{62,63} and among them is RFX2, a central regulator of post-meiotic spermatogenesis^{64,65}. Although
251 *Rfx2* is also not a direct target of KDM5C (Supplementary figure 1E), RFX2 mRNA is derepressed in *Kdm5c*-
252 KO EpiLCs (Figure 5J). Thus, RFX2 is a candidate transcription factor for driving the ectopic expression of
253 many KDM5C-unbound germline genes in *Kdm5c*-KO cells.

254 **KDM5C is recruited to CpG islands at germline promoters to facilitate *de novo* DNA
255 methylation**

256 Previous work found two germline gene promoters have a marked reduction in DNA CpG methylation
257 (CpGme) in the *Kdm5c*-KO adult hippocampus¹³. Since histone 3 lysine 4 di- and trimethylation (H3K4me2/3)
258 impede *de novo* CpGme^{66,67}, KDM5C's removal of H3K4me2/3 may be required to suppress germline
259 genes. However, KDM5C's catalytic activity was recently shown to be dispensable for suppressing *Dazl* in
260 undifferentiated ESCs⁴⁶. To reconcile these observations, we hypothesized KDM5C erases H3K4me2/3 to
261 promote the initial placement of CpGme at germline gene promoters in EpiLCs.

262 To test this hypothesis, we first characterized KDM5C's expression as naïve ESCs differentiate into
263 EpiLCs (Figure 6A). While *Kdm5c* mRNA steadily decreased from 0 to 48 hours of differentiation (Figure
264 6B), KDM5C protein initially increased from 0 to 24 hours but then decreased to near knockout levels by 48
265 hours (Figure 6C). We then characterized KDM5C's substrates (H3K4me2/3) at germline gene promoters
266 with *Kdm5c* loss using published ChIP-seq datasets^{22,42}. *Kdm5c*-KO samples showed a marked increase in
267 H3K4me2 in EpiLCs (Figure 6D) and H3K4me3 in the amygdala (Figure 6E) around the TSS of germline
268 genes. Together, these data suggest KDM5C acts during the transition between ESCs and EpiLCs to remove

269 H3K4me2/3 at germline gene promoters.
270 Germline genes accumulate CpG methylation (CpGme) at CpG islands (CGIs) during the transition
271 from naïve to primed pluripotency^{19,21,68}. We first examined how many of our germline-enriched genes had
272 promoter CGIs (TSS ± 500 bp) using the UCSC genome browser⁶⁹. Notably, out of 1,288 germline-enriched
273 genes, only 356 (27.64%) had promoter CGIs (Figure 6F). CGI-containing germline genes had higher
274 enrichment of meiotic gene ontologies compared to CGI-free genes, including meiotic nuclear division
275 (GO:0140013, p.adjust = 2.17e-12) and meiosis I (GO:0007127, p.adjust = 3.91e-10) (Figure 6G). Germline
276 genes with promoter CGIs were more highly expressed than CGI-free genes across spermatogenesis
277 stages, with highest expression in meiotic spermatocytes (Figure 6H). Contrastingly, CGI-free genes only
278 displayed substantial expression in post-meiotic round spermatids (Figure 6H). Although only a minor portion
279 of germline gene promoters contained CGIs, CGIs strongly determined KDM5C's recruitment to germline
280 genes ($p = 2.37e-67$, Odds Ratio = 17.8, Fisher's exact test), with 79.15% of KDM5C-bound germline gene
281 promoters harboring CGIs (Figure 6F).

282 To assess how KDM5C loss impacts initial CpGme placement at germline gene promoters, we performed
283 whole genome bisulfite sequencing (WGBS) in male wild-type and *Kdm5c*-KO ESCs and 96-hour extend
284 EpiLCs (exEpiLCs), when germline genes reach peak methylation levels¹⁸ (Figure 6I). We first identified
285 which germline gene promoters significantly gained CpGme in wild-type cells during nESC to exEpiLCs
286 differentiation (methylKit⁷⁰, $q < 0.01$, $|methylation\ difference| > 25\%$, TSS ± 500 bp). In wild-type cells, the
287 majority of germline genes gained substantial CpGme at their promoter during differentiation (60.08%),
288 regardless if their promoter contained a CGI (Figure 6J).

289 We then identified promoters differentially methylated in wild-type versus *Kdm5c*-KO exEpiLCs (methylKit,
290 $q < 0.01$, $|methylation\ difference| > 25\%$, TSS ± 500 bp). Of the 48,882 promoters assessed, 274 promoters
291 were significantly hypomethylated and 377 promoters were significantly hypermethylated with KDM5C loss
292 (Supplementary figure 2A). Many promoters hyper- and hypomethylated in *Kdm5c*-KO exEpiLCs belonged to
293 genes with unknown functions. Hypomethylated promoters were significantly enriched for germline gene
294 ontologies, such as meiotic nuclear division (GO:0140013, p.adjust = 0.012)(Supplementary figure 2B),
295 with 10.22% of hypomethylated promoters belonging to germline genes. Approximately half of germline
296 promoters hypomethylated in *Kdm5c*-KO exEpiLCs are direct targets of KDM5C in EpiLCs (13 out of 28
297 hypomethylated promoters).

298 Promoters that showed the most robust loss of CpGme in *Kdm5c*-KO exEpiLCs (lowest q-values) harbored
299 CGIs (Figure 6K). CGI promoters, but not CGI-free promoters, had a significant reduction in CpGme with
300 KDM5C loss as a whole (Figure 6L) (Non-CGI promoters $p = 0.0846$, CGI promoters $p = 0.0081$, Mann-
301 Whitney U test). Significantly hypomethylated promoters included germline genes consistently dysregulated
302 across multiple *Kdm5c*-KO RNA-seq datasets¹³, such as *D1Pas1* (methylation difference = -60.03%, q-value
303 = 3.26e-153) and *Naa11* (methylation difference = -42.45%, q-value = 1.44e-38) (Figure 6M). Surprisingly,
304 we found only a modest reduction in CpGme at *Dazl*'s promoter (methylation difference = -6.525%, q-value =

305 0.0159) (Figure 6N). Altogether, these results demonstrate KDM5C is recruited to germline gene CGIs in
306 EpiLCs to promote CpGme at germline gene promoters. Furthermore, this suggests while KDM5C's catalytic
307 activity is required for the repression of some germline genes, CpGme can be placed at others even with
308 elevated H3K4me2/3 around the TSS.

309 Discussion

310 In the above study, we demonstrate KDM5C's pivotal role in the development of tissue identity. We first
311 characterized tissue-enriched genes expressed within the mouse *Kdm5c*-KO brain and identified substantial
312 derepression of testis, liver, muscle, and ovary-enriched genes. Testis genes significantly enriched within the
313 *Kdm5c*-KO amygdala and hippocampus are specific to the germline and absent in somatic cells. *Kdm5c*-KO
314 epiblast-like cells (EpiLCs) aberrantly express key drivers of germline identity and meiosis, including *Dazl* and
315 *Stra8*, while the adult brain primarily expresses genes important for late spermatogenesis. We demonstrated
316 that although sex did not influence whether sperm or egg-specific genes were misexpressed, female EpiLCs
317 have heightened germline gene de-repression with KDM5C loss. Germline genes can become aberrantly
318 expressed in *Kdm5c*-KO cells via indirect mechanisms, such as activation through ectopic RFX transcription
319 factors. Finally, we found KDM5C is dynamically regulated during ESC to EpiLC differentiation to promote
320 long-term germline gene silencing through DNA methylation at CpG islands. Therefore, we propose KDM5C
321 plays a fundamental role in the development of tissue identity during early embryogenesis, including the
322 establishment of the soma-germline boundary. By systematically characterizing KDM5C's role in germline
323 gene repression, we unveiled unique mechanisms governing the misexpression of distinct germline gene
324 classes within somatic lineages. Ultimately, these data provide molecular footholds which can be exploited to
325 test the overarching contribution of ectopic germline gene expression upon neurodevelopment.

326 By comparing *Kdm5c* mutant males and females, we revealed germline gene suppression is sexually
327 dimorphic. While sex did not determine whether egg or sperm-specific genes were dysregulated, it greatly
328 influenced the degree of germline gene dysregulation. Female EpiLCs are more severely impacted by loss
329 of KDM5C-mediated germline gene suppression, yet this difference is not due to the increased number of
330 germline genes on the X chromosome^{53,54}. Increased germline gene misexpression in females may be
331 related to females having a higher dose of KDM5C than males, due to its escape from XCI^{49–52}. Intriguingly,
332 heterozygous knockout females (*Kdm5c*^{+/−}) also had over double the number of germline DEGs than
333 hemizygous knockout males (*Kdm5c*^{−/Y}), even though their expression of KDM5C should be roughly equivalent
334 to that of wild-type males (*Kdm5c*^{+/Y}). Males could partially compensate for KDM5C's loss via the Y-
335 chromosome homolog, KDM5D. However, KDM5D exhibits weaker demethylase activity than KDM5C⁸ and
336 has not been reported to regulate germline gene expression. Altogether, these results demonstrate germline
337 gene silencing mechanisms differ between males and females, which warrants further study to elucidate the
338 biological ramifications and underlying mechanisms.

339 We found KDM5C is largely dispensable for promoting normal gene expression during development, yet
340 is critical for suppressing ectopic developmental programs. It is important to note that while we highlighted
341 KDM5C's repression of germline genes, some germline-enriched genes like *Dazl* are also expressed at the 2-
342 cell stage and in naïve ESCs/the inner cell mass for their role in pluripotency and self-renewal^{41,46,71,72}. These
343 "self-renewal" germline genes are then silenced during ESC differentiation into epiblast stem cells/EpiLCs^{18,19}.
344 We found that while *Kdm5c*-KO EpiLCs express *Dazl*, they did not express 2-cell-specific genes like *Zscan4c*.
345 These data suggest the 2-cell-like state reported in *Kdm5c*-KO ESCs⁴⁶ likely reflects KDM5C's primary
346 role in germline gene repression. Germline gene misexpression in *Kdm5c*-KO EpiLCs may indicate they
347 are differentiating into primordial germ cell-like cells (PGCLCs)^{34,35,37}. Yet, *Kdm5c*-KO EpiLCs had normal
348 cellular morphology and properly expressed markers for primed pluripotency, including *Otx2* which blocks
349 EpiLC differentiation into PGCs/PGCLCs⁷³. In addition to unimpaired EpiLC differentiation, *Kdm5c*-KO gross
350 brain morphology is overall normal¹² and hardly any brain-specific genes were significantly dysregulated in
351 the amygdala and hippocampus. Thus, ectopic germline gene expression occurs in conjunction with overall
352 proper somatic differentiation in *Kdm5c*-KO animals.

353 Our work provides novel insight into the cross-talk between H3K4me2/3 and CpGme, which are gen-
354 erally mutually exclusive⁷⁴. In EpiLCs, loss of KDM5C binding at a subset of germline gene promoters,
355 e.g. *D1Pas1*, strongly impaired promoter CGI methylation and resulted in their long-lasting de-repression into
356 adulthood. Removal of H3K4me2/3 at CGIs is a plausible mechanism for KDM5C-mediated germline gene
357 suppression^{13,55}, given H3K4me2/3 can oppose DNMT3 activity^{66,67}. However, emerging work indicates
358 many histone-modifying enzymes have non-catalytic functions that influence gene expression, sometimes
359 even more potently than their catalytic roles^{75,76}. Indeed, KDM5C's catalytic activity was recently found to be
360 dispensible for repressing *Dazl* in ESCs⁴⁶. In our study, *Dazl*'s promoter still gained CpGme in *Kdm5c*-KO
361 exEpiLCs, even with elevated H3K4me2. *Dazl* and a few other germline genes employ multiple repressive
362 mechanisms to facilitate CpGme, such as DNMT3A/B recruitment via E2F6 and MGA^{17,18,47,48}. This suggests
363 alternative silencing mechanisms are sufficient to recruit DNMT3s to some germline CGIs, while others may
364 require KDM5C-mediated H3K4me removal to overcome promoter CGI escape from CpGme^{74,77}. These
365 results also suggest the requirement for KDM5C's catalytic activity can change depending upon the locus
366 and developmental stage, even for the same class of genes. However, further experiments are required to
367 determine if catalytically inactive KDM5C can suppress germline genes at later developmental stages.

368 By generating a comprehensive list of mouse germline-enriched genes, we were able to reveal distinct
369 derepressive mechanisms governing early versus late-stage germline developmental programs. Previous
370 work on germline gene silencing has focused on genes with promoter CGIs^{19,74}, and indeed the major-
371 ity of KDM5C targets in EpiLCs were germ cell identity genes harboring CGIs. However, over 70% of
372 germline-enriched gene promoters lacked CGIs, including the many KDM5C-unbound germline genes
373 that are de-repressed in *Kdm5c*-KO cells. CGI-free, KDM5C-unbound germline genes were primarily
374 late-stage spermatogenesis genes and significantly enriched for RFX2 binding sites, a central regulator

375 of spermiogenesis^{64,65}. These data suggest that once activated during early embryogenesis, drivers of
376 germline identity like *Rfx2*, *Stra8*, and *Dazl* turn on downstream germline programs, ultimately culminating in
377 the expression of spermiogenesis genes in the adult *Kdm5c*-KO brain. Therefore, we propose KDM5C is
378 recruited via promoter CGIs to act as a break against runaway activation of germline-specific programs.

379 The above work provides the mechanistic foundation for KDM5C-mediated repression of tissue and
380 germline-specific genes. However, the contribution of these ectopic, tissue-specific genes towards *Kdm5c*-
381 KO neurological impairments is still unknown. In addition to germline genes, we also identified significant
382 enrichment of muscle and liver-biased transcripts within the *Kdm5c*-KO brain. Intriguingly, select liver and
383 muscle-biased DEGs do have known roles within the brain, such as the liver-enriched lipid metabolism gene
384 *Apolipoprotein C-I (Apoc1)*²⁸. *APOC1* dysregulation is implicated in Alzheimer's disease in humans²⁹ and
385 overexpression of *Apoc1* in the mouse brain can impair learning and memory⁷⁸. KDM5C may therefore be
386 crucial for neurodevelopment by fine-tuning the expression of tissue-enriched, dosage-sensitive genes like
387 *Apoc1*.

388 Given that germline genes have no known functions within the brain, their impact upon neurodevelopment
389 is currently unknown. In *C. elegans*, somatic misexpression of germline genes via loss of *Retinoblastoma*
390 (*Rb*) homologs results in enhanced piRNA signaling and ectopic P granule formation in neurons^{79,80}. Ectopic
391 testicular germline transcripts have also been observed in a variety of cancers, including brain tumors in
392 *Drosophila* and mammals^{81,82} and shown to promote cancer progression⁸³⁻⁸⁵. Intriguingly, mouse models
393 and human cells for other chromatin-linked NDDs also display impaired soma-germline demarcation⁸⁶⁻⁸⁸,
394 such as mutations in DNA methyltransferase 3b (DNMT3B), H3K9me1/2 methyltransferases G9A/GLP,
395 and methyl-CpG -binding protein 2 (MECP2). Recently, the transcription factor ZMYM2 (ZNF198), whose
396 mutation causes neurodevelopmental-craniofacial syndrome with variable renal and cardiac abnormalities
397 (OMIM #619522), was also shown to repress germline genes by promoting H3K4 methylation removal and
398 CpGme⁸⁹. Thus, KDM5C is among a growing cohort of neurodevelopmental disorders that have erosion of
399 the germline-soma boundary. Further research is required to determine the impact of these germline genes
400 upon neuronal functions and the extent to which this phenomenon occurs in humans.

401 Materials and Methods

402 Classifying tissue-enriched and germline-enriched genes

403 Tissue-enriched differentially expressd genes (DEGs) were determined by their classification in a previ-
404 ously published dataset from 17 male and female mouse tissues²³. This study defined tissue expression as
405 greater than 1 Fragments Per Kilobase of transcript per Million mapped read (FPKM) and tissue enrichment
406 as at least 4-fold higher expression than any other tissue.

407 We curated a list of germline-enriched genes using an RNA-seq dataset from wild-type and germline-

408 depleted (*Kit*^{W/W^v}) male and female mouse embryos from embryonic day 12, 14, and 16³³, as well as adult
409 male testes³⁰. Germline-enriched genes met the following criteria: 1) their expression is greater than 1
410 FPKM in wild-type germline 2) their expression in any wild-type somatic tissues²³ does not exceed 20%
411 of maximum expression in wild-type germline, and 3) their expression in the germ cell-depleted (*Kit*^{W/W^v})
412 germline, for any sex or time point, does not exceed 20% of maximum expression in wild-type germline. We
413 defined sperm and egg-biased genes as those whose expression in the opposite sex, at any time point, is no
414 greater than 20% of the gene's maximum expression in a given sex. Genes that did not meet this threshold
415 for either sex were classified as 'unbiased'.

416 Cell culture

417 We utilized our previously established cultures of male wild-type and *Kdm5c* knockout (-KO)
418 embryonic stem cells⁴². Sex was confirmed by genotyping *Uba1/Uba1y* on the X and Y chromo-
419 somes with the following primers: 5'-TGGATGGTGTGCCAATG-3', 5'-CACCTGCACGTTGCCCTT-
420 3'. Deletion of *Kdm5c* exons 11 and 12, which destabilize KDM5C protein¹², was confirmed
421 through the primers 5'-ATGCCCATATTAAGAGTCCCTG-3', 5'-TCTGCCTTGATGGACTGTT-3', and
422 5'-GGTTCTAACACTCACATAGTG-3'.

423 Embryonic stem cells (ESCs) and epiblast-like cells were cultured using previously established
424 methods³⁸. Briefly, ESCs were initially cultured in primed ESC (pESC) media consisting of KnockOut
425 DMEM (Gibco#10829–018), fetal bovine serum (Gibco#A5209501), KnockOut serum replacement
426 (Invitrogen#10828–028), Glutamax (Gibco#35050-061), Anti-Anti (Gibco#15240-062), MEM Non-essential
427 amino acids (Gibco#11140-050), and beta-mercaptoethanol (Sigma#M7522). They were then transitioned
428 into ground-state, "naïve" ESCs (nESCs) by culturing for four passages in N2B27 media containing
429 DMEM/F12 (Gibco#11330–032), Neurobasal media (Gibco#21103–049), Gluamax (Gibco#35050-061),
430 Anti-Anti (Gibco#15240-062), N2 supplement (Invitrogen#17502048), and B27 supplement without vitamin
431 A (Invitrogen#12587-010), and beta-mercaptoethanol (Sigma#M7522). Both pESC and nESC media
432 were supplemented with 3 μ M GSK3 inhibitor CHIR99021 (Sigma #SML1046-5MG), 1 μ M MEK inhibitor
433 PD0325901 (Sigma #PZ0162-5MG), and 1,000 units/mL leukemia inhibitory factor (LIF, Millipore#ESG1107).

434 nESCs were differentiated into epiblast-like cells (EpiLCs, 48 hours) and extendend EpiLCs (exEpiLCs,
435 96 hours) by culturing in N2B27 media containing DMEM/F12, Neurobasal media, Gluamax, Anti-Anti, N2
436 supplement, B27 supplement (Invitrogen#17504044), and beta-mercaptoethanol supplemented with 10
437 ng/mL fibroblast growth factor 2 (FGF2, R&D Biotechne 233-FB), and 20 ng/mL activin A (R&D Biotechne
438 338AC050CF), as previously described³⁸.

439 **Real time quantitative PCR (RT-qPCR)**

440 nESCs were differentiated into EpiLCs as described above. Cells were lysed with Tri-reagent BD (Sigma
441 #T3809) at 0, 24, and 48 hours of differentiation. RNA was phase separated with 0.1 uL/uL 1-bromo-3-
442 chloropropane (Sigma #B9673) and then precipitated with isopropanol (Sigma #I9516) and ethanol puri-
443 fied. For each sample, 2 μ g of RNA was reverse transcribed using the ProtoScript II Reverse transcriptase kit
444 from New England Biolabs (NEB #M0368S) and primed with oligo dT. Expression of *Kdm5c* was detected us-
445 ing the primers 5'-CCCATGGAGGCCAGAGAATAAG-3' 5'-CTCAGCGGATAAGAGAATTGCTAC-3' and nor-
446 malized to TBP using the primers 5'-TTCAGAGGATGCTCTAGGGAAGA-3' 5'-CTGTGGAGTAAGTCCTGTGCC-
447 3' with the Power SYBR™ Green PCR Master Mix (ThermoFisher #4367659).

448 **Western Blot**

449 Total protein was extracted during nESC to EpiLC differentiation at 0, 24, and 48 hours by sonicating cells
450 at 20% amplitude for 15 seconds in 2X SDS sample buffer, then boiling at 100 °C for 10 minutes. Proteins
451 were separated on a 7.5% SDS page gel, transferred overnight onto a fluorescent membrane, blotted for
452 rabbit anti-KDM5C (in house, 1:500) and mouse anti-DAXX (Santa Cruz #(H-7): sc-8043, 1:500) and imaged
453 using the LiCor Odyssey CLx system. Band intensity was quantified using ImageJ.

454 **RNA sequencing (RNA-seq) data analysis**

455 After ensuring read quality via FastQC (v0.11.8), reads were then mapped to the mm10 *Mus musculus*
456 genome (Gencode) using STAR (v2.5.3a), during which we removed duplicates and kept only uniquely
457 mapped reads. Count files were generated by FeatureCounts (Subread v1.5.0), and BAM files were
458 converted to bigwigs using deeptools (v3.1.3) and visualized by the UCSC genome browser⁶⁹. RStudio
459 (v3.6.0) was then used to analyze counts files by DESeq2 (v1.26.0)²⁴ to identify differentially expressed
460 genes (DEGs) with a q-value (p-adjusted via FDR/Benjamini–Hochberg correction) less than 0.1 and a log2
461 fold change greater than 0.5. For all DESeq2 analyses, log2 fold changes were calculated with IfcShrink
462 using the ashR package⁹⁰. MA-plots were generated by ggpibr (v0.6.0), and Eulerr diagrams were generated
463 by eulerr (v6.1.1). Boxplots and scatterplots were generated by ggpibr (v0.6.0) and ggplot2 (v3.3.2). The
464 Upset plot was generated via the package UpSetR (v1.4.0)⁹¹. Gene ontology (GO) analyses were performed
465 by the R package enrichPlot (v1.16.2) using the biological processes setting and compareCluster.

466 **Chromatin immunoprecipitation followed by DNA sequencing (ChIP-seq) data analysis**

467 ChIP-seq reads were aligned to mm10 using Bowtie1 (v1.1.2) allowing up to two mismatches. Only
468 uniquely mapped reads were used for analysis. Peaks were called using MACS2 software (v2.2.9.1) using
469 input BAM files for normalization, with filters for a q-value < 0.1 and a fold enrichment > 1. We removed

470 “black-listed” genomic regions that often give aberrant signals. Common peak sets were obtained in R via
471 DiffBind⁹² (v3.6.5). In the case of KDM5C ChIP-seq, *Kdm5c*-KO peaks false-positive peaks were then
472 removed from wild-type samples using bedtools (v2.25.0). Peak proximity to genomic loci was determined
473 by ChIPSeeker⁹³ (v1.32.1). Gene ontology (GO) analyses were performed by the R package enrichPlot
474 (v1.16.2) using the biological processes setting and compareCluster. Enriched motifs were identified using
475 HOMER⁶⁰ to search for known motifs within 500 base pairs of the transcription start site. Average binding
476 across genes was visualized using deeptools (v3.1.3). Bigwigs were visualized using the UCSC genome
477 browser⁶⁹.

478 CpG island (CGI) analysis

479 Locations of CpG islands were determined through the mm10 UCSC genome browser CpG island track⁶⁹,
480 which classified CGIs as regions that have greater than 50% GC content, are larger than 200 base pairs,
481 and have a ratio of CG dinucleotides observed over the expected amount greater than 0.6. CGI genomic
482 coordinates were then annotated using ChIPseeker⁹³ (v1.32.1) and filtered for ones that lie within promoters
483 of germline-enriched genes (TSS ± 500).

484 Whole genome bisulfite sequencing (WGBS)

485 Genomic DNA (gDNA) from naïve ESCs and extended EpiLCs was extracted using the Wizard Genomic
486 DNA Purification Kit (Promega A1120), following the instructions for Tissue Culture Cells. gDNA from
487 two wild-types and two *Kdm5c*-KOs of each cell type was sent to Novogene for WGBS using the Illumina
488 NovaSeq X Plus platform and sequenced for 150bp paired-end reads (PE150). All samples had greater
489 than 99% bisulfite conversion rates. Reads were adapter and quality trimmed with Trim Galore (v0.6.10)
490 and aligned to the mm10 genome using Bismark⁹⁴ (v0.22.1). Analysis of differential methylation at germline
491 gene promoters was performed using methylKit⁷⁰ (v1.28.0) with a minimum coverage of 3 paired reads, a
492 percentage greater than 25% or less than -25%, and q-value less than 0.01. methylKit was also used to
493 calculate average percentage methylation at germline gene promoters. Methylation bedgraph tracks were
494 generated via Bismark and visualized using the UCSC genome browser⁶⁹.

495 Data availability

496 WGBS in wild-type and *Kdm5c*-KO ESCs and exEpiLCs

497 Raw fastq files are deposited in the Sequence Read Archive (SRA) <https://www.ncbi.nlm.nih.gov/sra>
498 under the bioProject XXX

499 **Published datasets**

500 All published datasets are available at the Gene Expression Omnibus (GEO) <https://www.ncbi.nlm.nih.gov/geo>. Published RNA-seq datasets analyzed in this study included the male wild-type and *Kdm5c*-KO
501 adult amygdala and hippocampus²² (available at GEO: GSE127722). Male and female wild-type, *Kdm5c*-KO,
502 and *Kdm5c*-HET EpiLCs⁴² are available at GEO: GSE96797.

504 Previously published ChIP-seq experiments included KDM5C binding in wild-type and *Kdm5c*-KO
505 EpiLCs⁴² (available at GEO: GSE96797) and mouse primary neuron cultures (PNCs) from the cortex
506 and hippocampus¹² (available at GEO: GSE61036). ChIP-seq of histone 3 lysine 4 dimethylation (H3K4me2)
507 in male wild-type and *Kdm5c*-KO EpiLCs⁴² is also available at GEO: GSE96797. ChIP-seq of histone 3 lysine
508 4 trimethylation (H3K4me3) in wild-type and *Kdm5c*-KO male amygdala²² are available at GEO: GSE127817.

509 **Data analysis**

510 Scripts used to generate the results, tables, and figures of this study are available via the GitHub
511 repository: XXX

512 **Acknowledgements**

513 We thank Drs. Sundeep Kalantry, Milan Samanta, and Rebecca Malcore for providing protocols and
514 expertise in culturing mouse ESCs and EpiLCs, as well as providing the wild-type and *Kdm5c*-KO ESCs
515 used in this study. We thank Dr. Jacob Mueller for his insight in germline gene regulation and directing us to
516 the germline-depleted mouse models. We also thank Drs. Gabriel Corfas, Kenneth Kwan, Natalie Tronson,
517 Michael Sutton, Stephanie Bielas, Donna Martin, and the members of the Iwase, Sutton, Bielas, and Martin
518 labs for helpful discussions and critiques of the data. We thank members of the University of Michigan
519 Reproductive Sciences Program for providing feedback throughout the development of this work. This work
520 was supported by grants from the National Institutes of Health (NIH) (National Institute of Neurological
521 Disorders and Stroke: NS089896, 5R21NS104774, and NS116008 to S.I.), Farrehi Family Foundation Grant
522 (to S.I.), the University of Michigan Career Training in Reproductive Biology (NIH T32HD079342, to K.M.B.),
523 the NIH Early Stage Training in the Neurosciences Training Grant (NIH T32NS076401 to K.M.B.), and the
524 Michigan Predoctoral Training in Genetics Grant (NIH T32GM007544, to I.V.)

525 **Author contributions**

526 K.M.B. and S.I. conceived the study and designed the experiments. I.V. generated the ESC and exEpiLC
527 WGBS data. K.M.B performed the data analysis and all other experiments. K.M.B and S.I. wrote and edited
528 the manuscript.

529 **References**

- 530 1. Strahl, B.D., and Allis, C.D. (2000). The language of covalent histone modifications. *Nature* **403**,
531 41–45. <https://doi.org/10.1038/47412>.
- 532 2. Jenuwein, T., and Allis, C.D. (2001). Translating the Histone Code. *Science* **293**, 1074–1080.
533 <https://doi.org/10.1126/science.1063127>.
- 534 3. Lewis, E.B. (1978). A gene complex controlling segmentation in *Drosophila*. *Nature* **276**, 565–570.
535 <https://doi.org/10.1038/276565a0>.
- 536 4. Kennison, J.A., and Tamkun, J.W. (1988). Dosage-dependent modifiers of polycomb and antennapedia
537 mutations in *Drosophila*. *Proc. Natl. Acad. Sci. U.S.A.* **85**, 8136–8140. <https://doi.org/10.1073/pnas.8>
538 5. Kassis, J.A., Kennison, J.A., and Tamkun, J.W. (2017). Polycomb and Trithorax Group Genes in
539 *Drosophila*. *Genetics* **206**, 1699–1725. <https://doi.org/10.1534/genetics.115.185116>.
- 540 6. Gabriele, M., Lopez Tobon, A., D'Agostino, G., and Testa, G. (2018). The chromatin basis of
541 neurodevelopmental disorders: Rethinking dysfunction along the molecular and temporal axes. *Prog
Neuropsychopharmacol Biol Psychiatry* **84**, 306–327. <https://doi.org/10.1016/j.pnpbp.2017.12.013>.
- 542 7. Schaefer, A., Sampath, S.C., Intrator, A., Min, A., Gertler, T.S., Surmeier, D.J., Tarakhovsky, A.,
543 and Greengard, P. (2009). Control of cognition and adaptive behavior by the GLP/G9a epigenetic
544 suppressor complex. *Neuron* **64**, 678–691. <https://doi.org/10.1016/j.neuron.2009.11.019>.
- 545 8. Iwase, S., Lan, F., Bayliss, P., De La Torre-Ubieta, L., Huarte, M., Qi, H.H., Whetstine, J.R., Bonni, A.,
546 Roberts, T.M., and Shi, Y. (2007). The X-Linked Mental Retardation Gene SMCX/JARID1C Defines a
547 Family of Histone H3 Lysine 4 Demethylases. *Cell* **128**, 1077–1088. <https://doi.org/10.1016/j.cell.200>
548 7.02.017.
- 549 9. Claes, S., Devriendt, K., Van Goethem, G., Roelen, L., Meireleire, J., Raeymaekers, P., Cassiman,
550 J.J., and Fryns, J.P. (2000). Novel syndromic form of X-linked complicated spastic paraparesia. *Am J
Med Genet* **94**, 1–4.
- 551 10. Jensen, L.R., Amende, M., Gurok, U., Moser, B., Gimmel, V., Tzschach, A., Janecke, A.R., Tariverdian,
552 G., Chelly, J., Fryns, J.P., et al. (2005). Mutations in the JARID1C gene, which is involved in
553 transcriptional regulation and chromatin remodeling, cause X-linked mental retardation. *Am J Hum
Genet* **76**, 227–236. <https://doi.org/10.1086/427563>.
- 554 11. Carmignac, V., Nambot, S., Lehalle, D., Callier, P., Moortgat, S., Benoit, V., Ghoumid, J., Delobel,
555 B., Smol, T., Thuillier, C., et al. (2020). Further delineation of the female phenotype with KDM5C
556 disease causing variants: 19 new individuals and review of the literature. *Clin Genet* **98**, 43–55.
557 <https://doi.org/10.1111/cge.13755>.

- 552 12. Iwase, S., Brookes, E., Agarwal, S., Badeaux, A.I., Ito, H., Vallianatos, C.N., Tomassy, G.S., Kasza, T.,
Lin, G., Thompson, A., et al. (2016). A Mouse Model of X-linked Intellectual Disability Associated with
Impaired Removal of Histone Methylation. *Cell Reports* *14*, 1000–1009. <https://doi.org/10.1016/j.celrep.2015.12.091>.
- 553
- 554 13. Scandaglia, M., Lopez-Atalaya, J.P., Medrano-Fernandez, A., Lopez-Cascales, M.T., Del Blanco, B.,
Lipinski, M., Benito, E., Olivares, R., Iwase, S., Shi, Y., et al. (2017). Loss of Kdm5c Causes Spurious
Transcription and Prevents the Fine-Tuning of Activity-Regulated Enhancers in Neurons. *Cell Rep* *21*,
47–59. <https://doi.org/10.1016/j.celrep.2017.09.014>.
- 555
- 556 14. Bonefas, K.M., Vallianatos, C.N., Raines, B., Tronson, N.C., and Iwase, S. (2023). Sexually Dimorphic
Alterations in the Transcriptome and Behavior with Loss of Histone Demethylase KDM5C. *Cells* *12*,
637. <https://doi.org/10.3390/cells12040637>.
- 557
- 558 15. Devlin, D.K., Ganley, A.R.D., and Takeuchi, N. (2023). A pan-metazoan view of germline-soma
distinction challenges our understanding of how the metazoan germline evolves. *Current Opinion in
Systems Biology* *36*, 100486. <https://doi.org/10.1016/j.coisb.2023.100486>.
- 559
- 560 16. Lehmann, R. (2012). Germline Stem Cells: Origin and Destiny. *Cell Stem Cell* *10*, 729–739.
<https://doi.org/10.1016/j.stem.2012.05.016>.
- 561
- 562 17. Endoh, M., Endo, T.A., Shinga, J., Hayashi, K., Farcas, A., Ma, K.W., Ito, S., Sharif, J., Endoh, T.,
Onaga, N., et al. (2017). PCGF6-PRC1 suppresses premature differentiation of mouse embryonic
stem cells by regulating germ cell-related genes. *eLife* *6*. <https://doi.org/10.7554/eLife.21064>.
- 563
- 564 18. Mochizuki, K., Sharif, J., Shirane, K., Uranishi, K., Bogutz, A.B., Janssen, S.M., Suzuki, A., Okuda,
A., Koseki, H., and Lorincz, M.C. (2021). Repression of germline genes by PRC1.6 and SETDB1
in the early embryo precedes DNA methylation-mediated silencing. *Nat Commun* *12*, 7020. <https://doi.org/10.1038/s41467-021-27345-x>.
- 565
- 566 19. Borgel, J., Guibert, S., Li, Y., Chiba, H., Schübeler, D., Sasaki, H., Forné, T., and Weber, M. (2010).
Targets and dynamics of promoter DNA methylation during early mouse development. *Nat Genet* *42*,
1093–1100. <https://doi.org/10.1038/ng.708>.
- 567
- 568 20. Velasco, G., Hubé, F., Rollin, J., Neuillet, D., Philippe, C., Bouzinba-Segard, H., Galvani, A., Viegas-
Péquignot, E., and Francastel, C. (2010). Dnmt3b recruitment through E2F6 transcriptional repressor
mediates germ-line gene silencing in murine somatic tissues. *Proc Natl Acad Sci U S A* *107*, 9281–
9286. <https://doi.org/10.1073/pnas.1000473107>.
- 569
- 570 21. Hackett, J.A., Reddington, J.P., Nestor, C.E., Dunican, D.S., Branco, M.R., Reichmann, J., Reik,
W., Surani, M.A., Adams, I.R., and Meehan, R.R. (2012). Promoter DNA methylation couples
genome-defence mechanisms to epigenetic reprogramming in the mouse germline. *Development*
139, 3623–3632. <https://doi.org/10.1242/dev.081661>.
- 571

- 572 22. Vallianatos, C.N., Raines, B., Porter, R.S., Bonefas, K.M., Wu, M.C., Garay, P.M., Collette, K.M.,
Seo, Y.A., Dou, Y., Keegan, C.E., et al. (2020). Mutually suppressive roles of KMT2A and KDM5C
in behaviour, neuronal structure, and histone H3K4 methylation. *Commun Biol* 3, 278. <https://doi.org/10.1038/s42003-020-1001-6>.
- 573
- 574 23. Li, B., Qing, T., Zhu, J., Wen, Z., Yu, Y., Fukumura, R., Zheng, Y., Gondo, Y., and Shi, L. (2017). A
Comprehensive Mouse Transcriptomic BodyMap across 17 Tissues by RNA-seq. *Sci Rep* 7, 4200.
<https://doi.org/10.1038/s41598-017-04520-z>.
- 575
- 576 24. Love, M.I., Huber, W., and Anders, S. (2014). Moderated estimation of fold change and dispersion for
577 RNA-seq data with DESeq2. *Genome Biol* 15, 550. <https://doi.org/10.1186/s13059-014-0550-8>.
- 578 25. Crackower, M.A., Kolas, N.K., Noguchi, J., Sarao, R., Kikuchi, K., Kaneko, H., Kobayashi, E., Kawai, Y.,
Kozieradzki, I., Landers, R., et al. (2003). Essential Role of Fkbp6 in Male Fertility and Homologous
579 Chromosome Pairing in Meiosis. *Science* 300, 1291–1295. <https://doi.org/10.1126/science.1083022>.
- 580 26. Xiol, J., Cora, E., Koglgruber, R., Chuma, S., Subramanian, S., Hosokawa, M., Reuter, M., Yang, Z.,
Berninger, P., Palencia, A., et al. (2012). A Role for Fkbp6 and the Chaperone Machinery in piRNA
Amplification and Transposon Silencing. *Molecular Cell* 47, 970–979. <https://doi.org/10.1016/j.molcel.2012.07.019>.
- 581
- 582 27. Cheng, S., Altmeppen, G., So, C., Welp, L.M., Penir, S., Ruhwedel, T., Menelaou, K., Harasimov, K.,
Stützer, A., Blayney, M., et al. (2022). Mammalian oocytes store mRNAs in a mitochondria-associated
583 membraneless compartment. *Science* 378, eabq4835. <https://doi.org/10.1126/science.abq4835>.
- 584 28. Rouland, A., Masson, D., Lagrost, L., Vergès, B., Gautier, T., and Bouillet, B. (2022). Role of
585 apolipoprotein C1 in lipoprotein metabolism, atherosclerosis and diabetes: A systematic review.
Cardiovasc Diabetol 21, 272. <https://doi.org/10.1186/s12933-022-01703-5>.
- 586 29. Leduc, V., Jasmin-Bélanger, S., and Poirier, J. (2010). APOE and cholesterol homeostasis in
587 Alzheimer's disease. *Trends in Molecular Medicine* 16, 469–477. <https://doi.org/10.1016/j.molmed.2010.07.008>.
- 588 30. Mueller, J.L., Skaletsky, H., Brown, L.G., Zaghlul, S., Rock, S., Graves, T., Auger, K., Warren,
W.C., Wilson, R.K., and Page, D.C. (2013). Independent specialization of the human and mouse X
589 chromosomes for the male germ line. *Nat Genet* 45, 1083–1087. <https://doi.org/10.1038/ng.2705>.
- 590 31. Handel, M.A., and Eppig, J.J. (1979). Sertoli Cell Differentiation in the Testes of Mice Genetically
Deficient in Germ Cells. *Biology of Reproduction* 20, 1031–1038. <https://doi.org/10.1095/biolreprod20.5.1031>.
- 591
- 592 32. Green, C.D., Ma, Q., Manske, G.L., Shami, A.N., Zheng, X., Marini, S., Moritz, L., Sultan, C.,
Gurczynski, S.J., Moore, B.B., et al. (2018). A Comprehensive Roadmap of Murine Spermatogenesis
Defined by Single-Cell RNA-Seq. *Dev Cell* 46, 651–667.e10. <https://doi.org/10.1016/j.devcel.2018.07.025>.
- 593

- 594 33. Soh, Y.Q., Junker, J.P., Gill, M.E., Mueller, J.L., van Oudenaarden, A., and Page, D.C. (2015). A
Gene Regulatory Program for Meiotic Prophase in the Fetal Ovary. *PLoS Genet* *11*, e1005531.
<https://doi.org/10.1371/journal.pgen.1005531>.
- 595
- 596 34. Magnúsdóttir, E., and Surani, M.A. (2014). How to make a primordial germ cell. *Development* *141*,
245–252. <https://doi.org/10.1242/dev.098269>.
- 597
- 598 35. Günesdogan, U., Magnúsdóttir, E., and Surani, M.A. (2014). Primordial germ cell specification: A
context-dependent cellular differentiation event [corrected]. *Philos Trans R Soc Lond B Biol Sci* *369*.
<https://doi.org/10.1098/rstb.2013.0543>.
- 599
- 600 36. Bardot, E.S., and Hadjantonakis, A.-K. (2020). Mouse gastrulation: Coordination of tissue patterning,
specification and diversification of cell fate. *Mechanisms of Development* *163*, 103617. <https://doi.org/10.1016/j.mod.2020.103617>.
- 601
- 602 37. Hayashi, K., Ohta, H., Kurimoto, K., Aramaki, S., and Saitou, M. (2011). Reconstitution of the
mouse germ cell specification pathway in culture by pluripotent stem cells. *Cell* *146*, 519–532.
<https://doi.org/10.1016/j.cell.2011.06.052>.
- 603
- 604 38. Samanta, M., and Kalantry, S. (2020). Generating primed pluripotent epiblast stem cells: A methodol-
ogy chapter. *Curr Top Dev Biol* *138*, 139–174. <https://doi.org/10.1016/bs.ctdb.2020.01.005>.
- 605
- 606 39. Welling, M., Chen, H., Muñoz, J., Musheev, M.U., Kester, L., Junker, J.P., Mischerikow, N., Arbab, M.,
Kuijk, E., Silberstein, L., et al. (2015). DAZL regulates Tet1 translation in murine embryonic stem cells.
EMBO Reports *16*, 791–802. <https://doi.org/10.15252/embr.201540538>.
- 607
- 608 40. Macfarlan, T.S., Gifford, W.D., Driscoll, S., Lettieri, K., Rowe, H.M., Bonanomi, D., Firth, A., Singer, O.,
Trono, D., and Pfaff, S.L. (2012). Embryonic stem cell potency fluctuates with endogenous retrovirus
activity. *Nature* *487*, 57–63. <https://doi.org/10.1038/nature11244>.
- 609
- 610 41. Suzuki, A., Hirasaki, M., Hishida, T., Wu, J., Okamura, D., Ueda, A., Nishimoto, M., Nakachi, Y.,
Mizuno, Y., Okazaki, Y., et al. (2016). Loss of MAX results in meiotic entry in mouse embryonic and
germline stem cells. *Nat Commun* *7*, 11056. <https://doi.org/10.1038/ncomms11056>.
- 611
- 612 42. Samanta, M.K., Gayen, S., Harris, C., Maclary, E., Murata-Nakamura, Y., Malcore, R.M., Porter, R.S.,
Garay, P.M., Vallianatos, C.N., Samollow, P.B., et al. (2022). Activation of Xist by an evolutionarily
conserved function of KDM5C demethylase. *Nat Commun* *13*, 2602. [https://doi.org/10.1038/s41467-022-30352-1](https://doi.org/10.1038/s41467-
022-30352-1).
- 613
- 614 43. Koubova, J., Menke, D.B., Zhou, Q., Capel, B., Griswold, M.D., and Page, D.C. (2006). Retinoic
acid regulates sex-specific timing of meiotic initiation in mice. *Proc. Natl. Acad. Sci. U.S.A.* *103*,
2474–2479. <https://doi.org/10.1073/pnas.0510813103>.
- 615

- 616 44. Lin, Y., Gill, M.E., Koubova, J., and Page, D.C. (2008). Germ Cell-Intrinsic and -Extrinsic Factors
617 Govern Meiotic Initiation in Mouse Embryos. *Science* *322*, 1685–1687. <https://doi.org/10.1126/science.1166340>.
- 618 45. Endo, T., Mikedis, M.M., Nicholls, P.K., Page, D.C., and De Rooij, D.G. (2019). Retinoic Acid and Germ
619 Cell Development in the Ovary and Testis. *Biomolecules* *9*, 775. <https://doi.org/10.3390/biom9120775>.
- 620 46. Gupta, N., Yakhou, L., Albert, J.R., Azogui, A., Ferry, L., Kirsh, O., Miura, F., Battault, S., Yamaguchi,
621 K., Laisné, M., et al. (2023). A genome-wide screen reveals new regulators of the 2-cell-like cell state.
Nat Struct Mol Biol. <https://doi.org/10.1038/s41594-023-01038-z>.
- 622 47. Pohlers, M., Truss, M., Frede, U., Scholz, A., Strehle, M., Kuban, R.-J., Hoffmann, B., Morkel, M.,
623 Birchmeier, C., and Hagemeier, C. (2005). A Role for E2F6 in the Restriction of Male-Germ-Cell-
Specific Gene Expression. *Current Biology* *15*, 1051–1057. <https://doi.org/10.1016/j.cub.2005.04.060>.
- 624 48. Dahlet, T., Truss, M., Frede, U., Al Adhami, H., Bardet, A.F., Dumas, M., Vallet, J., Chicher, J.,
625 Hammann, P., Kottnik, S., et al. (2021). E2F6 initiates stable epigenetic silencing of germline genes
during embryonic development. *Nat Commun* *12*, 3582. <https://doi.org/10.1038/s41467-021-23596-w>.
- 626 49. Agulnik, A.I., Mitchell, M.J., Mattei, M.G., Borsani, G., Avner, P.A., Lerner, J.L., and Bishop, C.E.
627 (1994). A novel X gene with a widely transcribed Y-linked homologue escapes X-inactivation in mouse
and human. *Hum Mol Genet* *3*, 879–884. <https://doi.org/10.1093/hmg/3.6.879>.
- 628 50. Carrel, L., Hunt, P.A., and Willard, H.F. (1996). Tissue and lineage-specific variation in inactive
629 X chromosome expression of the murine Smcx gene. *Hum Mol Genet* *5*, 1361–1366. <https://doi.org/10.1093/hmg/5.9.1361>.
- 630 51. Sheardown, S., Norris, D., Fisher, A., and Brockdorff, N. (1996). The mouse Smcx gene exhibits
631 developmental and tissue specific variation in degree of escape from X inactivation. *Hum Mol Genet*
5, 1355–1360. <https://doi.org/10.1093/hmg/5.9.1355>.
- 632 52. Xu, J., Deng, X., and Disteche, C.M. (2008). Sex-Specific Expression of the X-Linked Histone
633 Demethylase Gene Jarid1c in Brain. *PLoS ONE* *3*, e2553. <https://doi.org/10.1371/journal.pone.0002553>.
- 634 53. Wang, P.J., McCarrey, J.R., Yang, F., and Page, D.C. (2001). An abundance of X-linked genes
635 expressed in spermatogonia. *Nat Genet* *27*, 422–426. <https://doi.org/10.1038/86927>.
- 636 54. Khil, P.P., Smirnova, N.A., Romanienko, P.J., and Camerini-Otero, R.D. (2004). The mouse X
chromosome is enriched for sex-biased genes not subject to selection by meiotic sex chromosome
637 inactivation. *Nat Genet* *36*, 642–646. <https://doi.org/10.1038/ng1368>.

- 638 55. Al Adhami, H., Vallet, J., Schaal, C., Schumacher, P., Bardet, A.F., Dumas, M., Chicher, J., Hammann, P., Daujat, S., and Weber, M. (2023). Systematic identification of factors involved in the silencing
639 of germline genes in mouse embryonic stem cells. *Nucleic Acids Research* *51*, 3130–3149. <https://doi.org/10.1093/nar/gkad071>.
- 640 56. Hurlin, P.J. (1999). Mga, a dual-specificity transcription factor that interacts with Max and contains a
641 T-domain DNA-binding motif. *The EMBO Journal* *18*, 7019–7028. <https://doi.org/10.1093/emboj/18.2.4.7019>.
- 642 57. Tatsumi, D., Hayashi, Y., Endo, M., Kobayashi, H., Yoshioka, T., Kiso, K., Kanno, S., Nakai, Y., Maeda, I., Mochizuki, K., et al. (2018). DNMTs and SETDB1 function as co-repressors in MAX-mediated
643 repression of germ cell-related genes in mouse embryonic stem cells. *PLoS ONE* *13*, e0205969.
<https://doi.org/10.1371/journal.pone.0205969>.
- 644 58. Stielow, B., Finkernagel, F., Stiewe, T., Nist, A., and Suske, G. (2018). MGA, L3MBTL2 and E2F6
645 determine genomic binding of the non-canonical Polycomb repressive complex PRC1.6. *PLoS Genet*
14, e1007193. <https://doi.org/10.1371/journal.pgen.1007193>.
- 646 59. Tahiliani, M., Mei, P., Fang, R., Leonor, T., Rutenberg, M., Shimizu, F., Li, J., Rao, A., and Shi, Y.
647 (2007). The histone H3K4 demethylase SMCX links REST target genes to X-linked mental retardation.
Nature *447*, 601–605. <https://doi.org/10.1038/nature05823>.
- 648 60. Heinz, S., Benner, C., Spann, N., Bertolino, E., Lin, Y.C., Laslo, P., Cheng, J.X., Murre, C., Singh, H.,
649 and Glass, C.K. (2010). Simple Combinations of Lineage-Determining Transcription Factors Prime
cis-Regulatory Elements Required for Macrophage and B Cell Identities. *Molecular Cell* *38*, 576–589.
<https://doi.org/10.1016/j.molcel.2010.05.004>.
- 650 61. Gajiwala, K.S., Chen, H., Cornille, F., Roques, B.P., Reith, W., Mach, B., and Burley, S.K. (2000).
651 Structure of the winged-helix protein hRFX1 reveals a new mode of DNA binding. *Nature* *403*,
916–921. <https://doi.org/10.1038/35002634>.
- 652 62. Swoboda, P., Adler, H.T., and Thomas, J.H. (2000). The RFX-Type Transcription Factor DAF-19
653 Regulates Sensory Neuron Cilium Formation in *C. elegans*. *Molecular Cell* *5*, 411–421. [https://doi.org/10.1016/S1097-2765\(00\)80436-0](https://doi.org/10.1016/S1097-2765(00)80436-0).
- 654 63. Ashique, A.M., Choe, Y., Karlen, M., May, S.R., Phamluong, K., Solloway, M.J., Ericson, J., and
655 Peterson, A.S. (2009). The Rfx4 Transcription Factor Modulates Shh Signaling by Regional Control of
Ciliogenesis. *Sci. Signal.* *2*. <https://doi.org/10.1126/scisignal.2000602>.
- 656 64. Kistler, W.S., Baas, D., Lemeille, S., Paschaki, M., Seguin-Estevez, Q., Barras, E., Ma, W., Duteyrat, J.-L., Morlé, L., Durand, B., et al. (2015). RFX2 Is a Major Transcriptional Regulator of Spermiogenesis.
657 *PLoS Genet* *11*, e1005368. <https://doi.org/10.1371/journal.pgen.1005368>.

- 658 65. Wu, Y., Hu, X., Li, Z., Wang, M., Li, S., Wang, X., Lin, X., Liao, S., Zhang, Z., Feng, X., et al.
659 (2016). Transcription Factor RFX2 Is a Key Regulator of Mouse Spermiogenesis. *Sci Rep* 6, 20435.
<https://doi.org/10.1038/srep20435>.
- 660 66. Otani, J., Nankumo, T., Arita, K., Inamoto, S., Ariyoshi, M., and Shirakawa, M. (2009). Structural basis
661 for recognition of H3K4 methylation status by the DNA methyltransferase 3A ATRX–DNMT3–DNMT3L
domain. *EMBO Reports* 10, 1235–1241. <https://doi.org/10.1038/embor.2009.218>.
- 662 67. Guo, X., Wang, L., Li, J., Ding, Z., Xiao, J., Yin, X., He, S., Shi, P., Dong, L., Li, G., et al. (2015).
663 Structural insight into autoinhibition and histone H3-induced activation of DNMT3A. *Nature* 517,
640–644. <https://doi.org/10.1038/nature13899>.
- 664 68. Meissner, A., Mikkelsen, T.S., Gu, H., Wernig, M., Hanna, J., Sivachenko, A., Zhang, X., Bernstein,
665 B.E., Nusbaum, C., Jaffe, D.B., et al. (2008). Genome-scale DNA methylation maps of pluripotent and
differentiated cells. *Nature* 454, 766–770. <https://doi.org/10.1038/nature07107>.
- 666 69. Nassar, L.R., Barber, G.P., Benet-Pagès, A., Casper, J., Clawson, H., Diekhans, M., Fischer, C.,
Gonzalez, J.N., Hinrichs, A.S., Lee, B.T., et al. (2023). The UCSC Genome Browser database: 2023
667 update. *Nucleic Acids Research* 51, D1188–D1195. <https://doi.org/10.1093/nar/gkac1072>.
- 668 70. Akalin, A., Kormaksson, M., Li, S., Garrett-Bakelman, F.E., Figueiroa, M.E., Melnick, A., and Mason,
C.E. (2012). methylKit: A comprehensive R package for the analysis of genome-wide DNA methylation
669 profiles. *Genome Biol* 13, R87. <https://doi.org/10.1186/gb-2012-13-10-r87>.
- 670 71. Torres-Padilla, M.-E. (2020). On transposons and totipotency. *Philos Trans R Soc Lond B Biol Sci*
671 375, 20190339. <https://doi.org/10.1098/rstb.2019.0339>.
- 672 72. Yang, M., Yu, H., Yu, X., Liang, S., Hu, Y., Luo, Y., Izsvák, Z., Sun, C., and Wang, J. (2022). Chemical-
induced chromatin remodeling reprograms mouse ESCs to totipotent-like stem cells. *Cell Stem Cell*
673 29, 400–418.e13. <https://doi.org/10.1016/j.stem.2022.01.010>.
- 674 73. Zhang, J., Zhang, M., Acampora, D., Vojtek, M., Yuan, D., Simeone, A., and Chambers, I. (2018).
OTX2 restricts entry to the mouse germline. *Nature* 562, 595–599. [018-0581-5](https://doi.org/10.1038/s41586-
675 018-0581-5).
- 676 74. Weber, M., Hellmann, I., Stadler, M.B., Ramos, L., Pääbo, S., Rebhan, M., and Schübeler, D. (2007).
Distribution, silencing potential and evolutionary impact of promoter DNA methylation in the human
677 genome. *Nat Genet* 39, 457–466. <https://doi.org/10.1038/ng1990>.
- 678 75. Aubert, Y., Egolf, S., and Capell, B.C. (2019). The Unexpected Noncatalytic Roles of Histone Modifiers
in Development and Disease. *Trends in Genetics* 35, 645–657. <https://doi.org/10.1016/j.tig.2019.06.004>.

- 680 76. Morgan, M.A.J., and Shilatifard, A. (2020). Reevaluating the roles of histone-modifying enzymes
and their associated chromatin modifications in transcriptional regulation. *Nat Genet* 52, 1271–1281.
<https://doi.org/10.1038/s41588-020-00736-4>.
- 681
- 682 77. Long, H.K., King, H.W., Patient, R.K., Odom, D.T., and Klose, R.J. (2016). Protection of CpG
islands from DNA methylation is DNA-encoded and evolutionarily conserved. *Nucleic Acids Res* 44,
6693–6706. <https://doi.org/10.1093/nar/gkw258>.
- 683
- 684 78. Abildayeva, K., Berbée, J.F.P., Blokland, A., Jansen, P.J., Hoek, F.J., Meijer, O., Lütjohann, D., Gautier,
T., Pillot, T., De Vente, J., et al. (2008). Human apolipoprotein C-I expression in mice impairs learning
and memory functions. *Journal of Lipid Research* 49, 856–869. <https://doi.org/10.1194/jlr.M700518JLR200>.
- 685
- 686 79. Wang, D., Kennedy, S., Conte, D., Kim, J.K., Gabel, H.W., Kamath, R.S., Mello, C.C., and Ruvkun,
G. (2005). Somatic misexpression of germline P granules and enhanced RNA interference in
retinoblastoma pathway mutants. *Nature* 436, 593–597. <https://doi.org/10.1038/nature04010>.
- 687
- 688 80. Wu, X., Shi, Z., Cui, M., Han, M., and Ruvkun, G. (2012). Repression of germline RNAi pathways
in somatic cells by retinoblastoma pathway chromatin complexes. *PLoS Genet* 8, e1002542. <https://doi.org/10.1371/journal.pgen.1002542>.
- 689
- 690 81. Nielsen, A.Y., and Gjerstorff, M.F. (2016). Ectopic Expression of Testis Germ Cell Proteins in Cancer
and Its Potential Role in Genomic Instability. *Int J Mol Sci* 17. <https://doi.org/10.3390/ijms17060890>.
- 691
- 692 82. Adebayo Babatunde, K., Najafi, A., Salehipour, P., Modarressi, M.H., and Mobasheri, M.B. (2017).
Cancer/Testis genes in relation to sperm biology and function. *Iranian Journal of Basic Medical
Sciences* 20. <https://doi.org/10.22038/ijbms.2017.9259>.
- 693
- 694 83. Janic, A., Mendizabal, L., Llamazares, S., Rossell, D., and Gonzalez, C. (2010). Ectopic expression
of germline genes drives malignant brain tumor growth in *Drosophila*. *Science* 330, 1824–1827.
<https://doi.org/10.1126/science.1195481>.
- 695
- 696 84. Ghafouri-Fard, S., and Modarressi, M.-H. (2012). Expression of Cancer–Testis Genes in Brain Tumors:
Implications for Cancer Immunotherapy. *Immunotherapy* 4, 59–75. <https://doi.org/10.2217/imt.11.145>.
- 697
- 698 85. Nin, D.S., and Deng, L.-W. (2023). Biology of Cancer-Testis Antigens and Their Therapeutic Implications
in Cancer. *Cells* 12, 926. <https://doi.org/10.3390/cells12060926>.
- 699
- 700 86. Bonefas, K.M., and Iwase, S. (2021). Soma-to-germline transformation in chromatin-linked neurode-
velopmental disorders? *FEBS J.* <https://doi.org/10.1111/febs.16196>.
- 701
- 702 87. Velasco, G., Walton, E.L., Sterlin, D., Hédouin, S., Nitta, H., Ito, Y., Fouyssac, F., Mégarbané, A.,
Sasaki, H., Picard, C., et al. (2014). Germline genes hypomethylation and expression define a
molecular signature in peripheral blood of ICF patients: Implications for diagnosis and etiology.
Orphanet J Rare Dis 9, 56. <https://doi.org/10.1186/1750-1172-9-56>.
- 703

- 704 88. Walton, E.L., Francastel, C., and Velasco, G. (2014). Dnmt3b Prefers Germ Line Genes and Cen-
705 tromeric Regions: Lessons from the ICF Syndrome and Cancer and Implications for Diseases. *Biology*
706 (Basel) 3, 578–605. <https://doi.org/10.3390/biology3030578>.
- 707 89. Graham-Paquin, A.-L., Saini, D., Sirois, J., Hossain, I., Katz, M.S., Zhuang, Q.K.-W., Kwon, S.Y.,
708 Yamanaka, Y., Bourque, G., Bouchard, M., et al. (2023). ZMYM2 is essential for methylation of
709 germline genes and active transposons in embryonic development. *Nucleic Acids Research*, gkad540.
<https://doi.org/10.1093/nar/gkad540>.
- 710 90. Stephens, M. (2016). False discovery rates: A new deal. *Biostat*, kxw041. <https://doi.org/10.1093/biostatistics/kxw041>.
- 711 91. Conway, J.R., Lex, A., and Gehlenborg, N. (2017). UpSetR: An R package for the visualization of
712 intersecting sets and their properties. *Bioinformatics* 33, 2938–2940. <https://doi.org/10.1093/bioinformatics/btx364>.
- 713 92. Ross-Innes, C.S., Stark, R., Teschendorff, A.E., Holmes, K.A., Ali, H.R., Dunning, M.J., Brown, G.D.,
714 Gojis, O., Ellis, I.O., Green, A.R., et al. (2012). Differential oestrogen receptor binding is associated
715 with clinical outcome in breast cancer. *Nature* 481, 389–393. <https://doi.org/10.1038/nature10730>.
- 716 93. Yu, G., Wang, L.G., and He, Q.Y. (2015). ChIPseeker: An R/Bioconductor package for ChIP peak
717 annotation, comparison and visualization. *Bioinformatics* 31, 2382–2383. <https://doi.org/10.1093/bioinformatics/btv145>.
- 718 94. Krueger, F., and Andrews, S.R. (2011). Bismark: A flexible aligner and methylation caller for Bisulfite-
719 Seq applications. *Bioinformatics* 27, 1571–1572. <https://doi.org/10.1093/bioinformatics/btr167>.

718 **Figures and Tables**

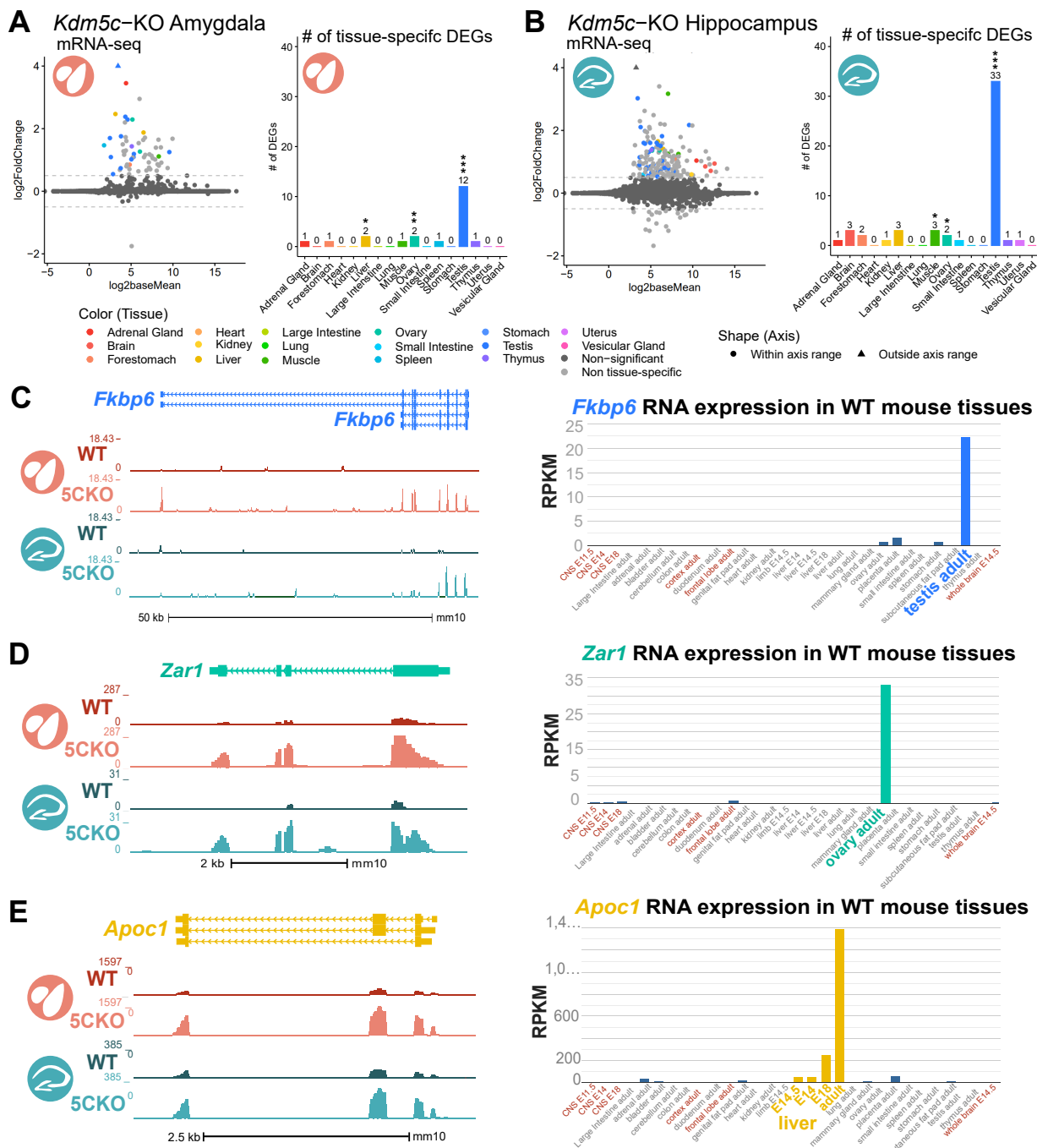


Figure 1: Tissue-enriched genes are misexpressed in the *Kdm5c*-KO brain. **A-B.** Expression of tissue-enriched genes (Li et al 2017) in the male *Kdm5c*-KO amygdala (A) and hippocampus (B). Left - MA plot of mRNA-sequencing. Right - Number of tissue-enriched differentially expressed genes (DEGs). * p<0.05, ** p<0.01, *** p<0.001, Fisher's exact test. **C.** Left - UCSC browser view of an example aberrantly expressed testis-enriched DEG, *FK506 binding protein 6* (*Fkbp6*) in the wild-type (WT) and *Kdm5c*-KO (5CKO) amygdala (red) and hippocampus (teal) (Average, n = 4). Right - Expression of *Cyct* in wild-type tissues from NCBI Gene, with testis highlighted in blue and brain tissues highlighted in red. **D.** Left - UCSC browser view of an example ovary-enriched DEG, *Zygotic arrest 1* (*Zar1*). Right - Expression of *Zar1* in wild-type tissues from NCBI Gene, with ovary highlighted in teal and brain tissues highlighted in red. **E.** Left - UCSC browser view of an example liver-enriched DEG, *Apolipoprotein C-I* (*Apoc1*). Right - Expression of *Apoc1* in wild-type tissues from NCBI Gene, with liver highlighted in orange and brain tissues highlighted in red.

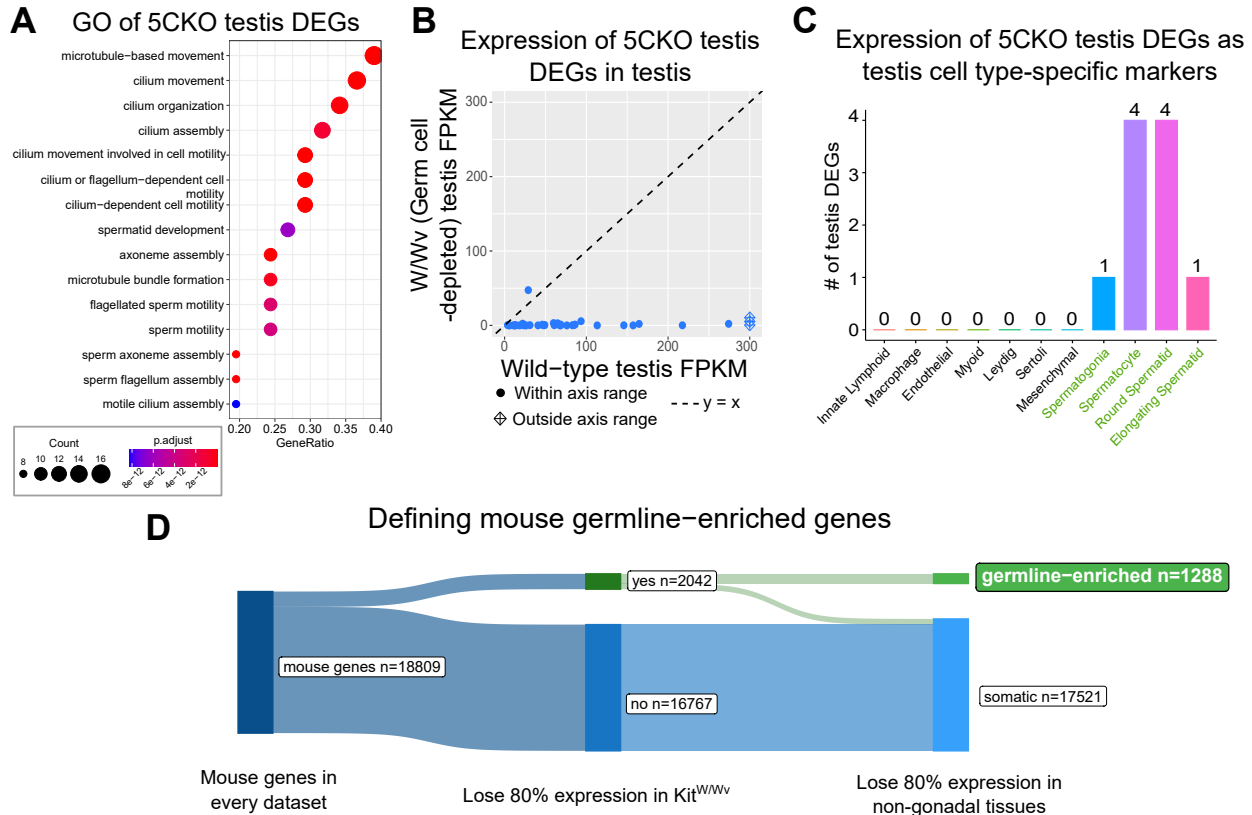


Figure 2: Aberrant transcription of germline genes in the *Kdm5c*-KO in the brain. **A.** enrichPlot gene ontology (GO) of *Kdm5c*-KO amygdala and hippocampus testis-enriched DEGs **B.** Expression of testis DEGs in wild-type (WT) testis versus germ cell-depleted (W/Wv) testis (Mueller et al 2013). Expression is in Fragments Per Kilobase of transcript per Million mapped reads (FPKM). **C.** Number of testis DEGs that were classified as cell-type specific markers in a single cell RNA-seq dataset of the testis (Green et al 2018). Germline cell types are highlighted in green, somatic cell types in black. **D.** Sankey diagram of mouse genes filtered for germline enrichment based on their expression in wild-type and W/Wv mice and in adult mouse non-gonadal tissues (Li et al 2017).

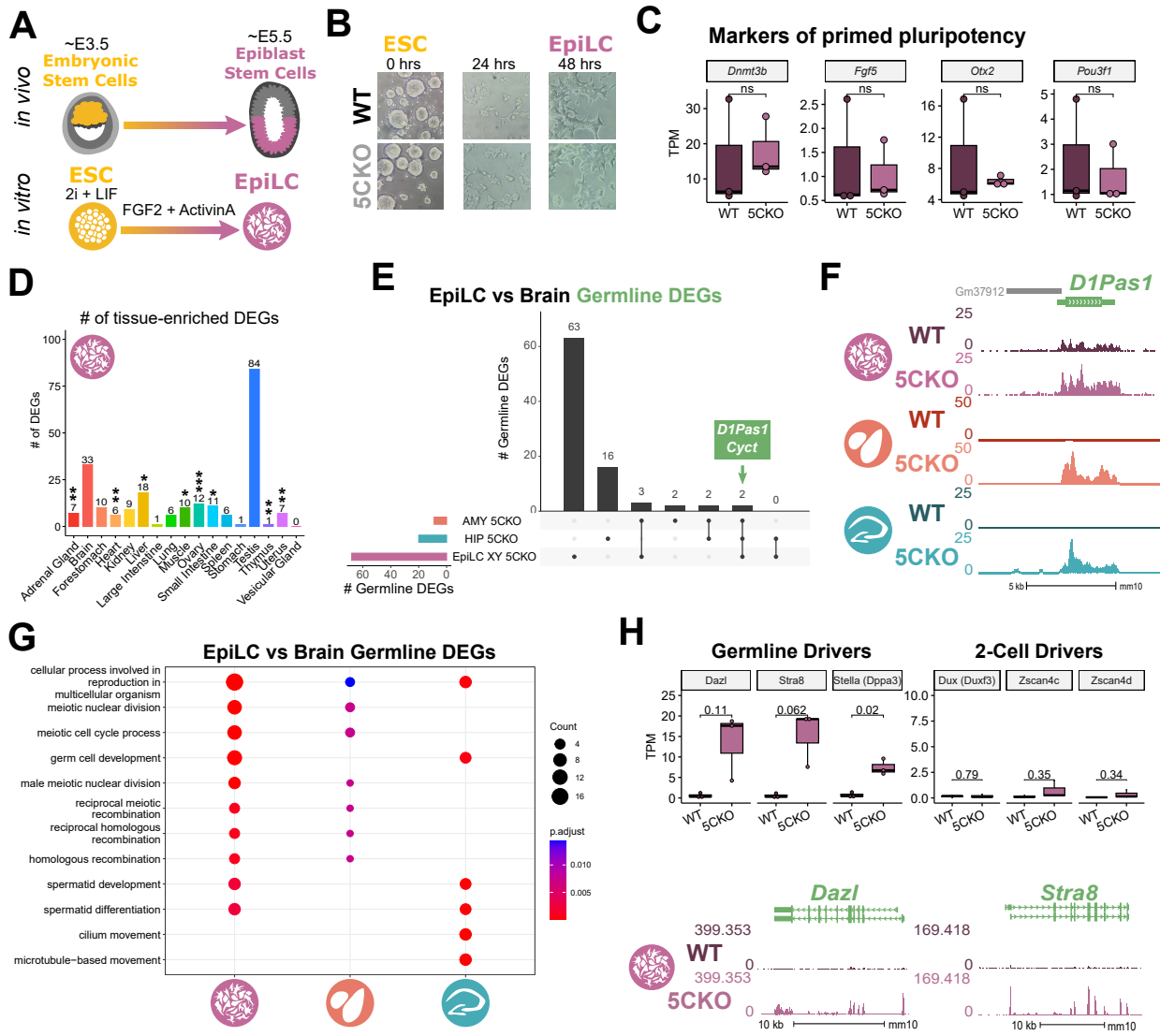


Figure 3: Kdm5c-KO epiblast-like cells express key drivers of germline identity **A.** Top - Diagram of *in vivo* differentiation of embryonic stem cells (ESCs) of the inner cell mass into epiblast stem cells. Bottom - *in vitro* differentiation of ESCs into epiblast-like cells (EpiLCs). **B.** Representative images of male wild-type (WT) and *Kdm5c*-KO (5CKO) cells during ESC to EpiLC differentiation. Brightfield images taken at 20X. **C.** No significant difference in primed pluripotency marker expression in wild-type versus *Kdm5c*-KO EpiLCs. Welch's t-test, expression in transcripts per million (TPM). **D.** Number of tissue-enriched differentially expressed genes (DEGs) in *Kdm5c*-KO EpiLCs. * $p < 0.05$, ** $p < 0.01$, *** $p < 0.001$, Fisher's exact test. **E.** Upset plot displaying the overlap of germline DEGs expressed in *Kdm5c*-KO EpiLCs, amygdala (AMY), and hippocampus (HIP) RNA-seq datasets. **F.** UCSC browser view of an example germline gene, *D1Pas1*, that is dysregulated *Kdm5c*-KO EpiLCs (top, purple. Average, $n = 3$), amygdala (middle, red. Average, $n = 4$), and hippocampus (bottom, blue. Average, $n = 4$). **G.** enrichPlot gene ontology analysis comparing enriched biological processes for *Kdm5c*-KO EpiLC, amygdala, and hippocampus germline DEGs. **H.** Top left - Example germline identity DEGs unique to EpiLCs. Top right - Example 2-cell genes that are not dysregulated in *Kdm5c*-KO EpiLCs. p-values for Welch's t-test. Bottom - UCSC browser view of *Dazl* and *Stra8* expression in wild-type and *Kdm5c*-KO EpiLCs (Average, $n = 3$).

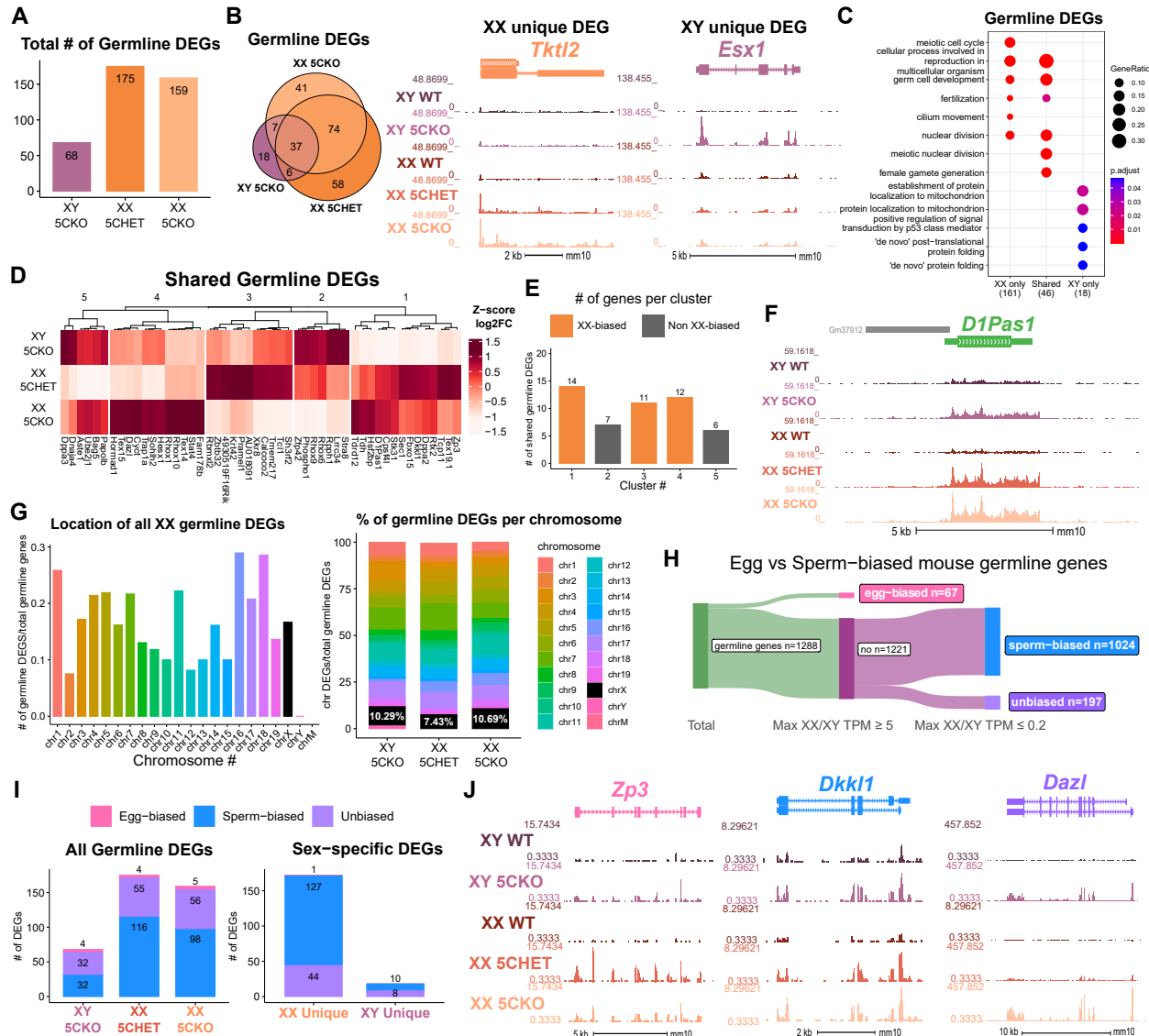


Figure 4: Chromosomal sex influences *Kdm5c*-KO germline gene misexpression. **A.** Total number of germline-enriched RNA-seq DEGs for male hemizygous *Kdm5c* knockout EpilCs (XY 5CKO, purple), female heterozygous *Kdm5c* knockout (XX 5CHET, orange), female homozygous *Kdm5c* knockout (XX 5CKO, light orange) EpilCs. **B.** Left - Eulerr overlap of *Kdm5c* mutant male and female EpilC germline DEGs. Right - Example of germline DEGs unique to females or males, *Tktl2* and *Esx1*. **C.** enrichPlot gene ontology analysis comparing enriched biological processes for germline DEGs shared between *Kdm5c* mutant males and females, or unique to one sex (XX only or XY only). **D.** Heatmap of germline DEGs shared between male and female mutants. Color is the average log 2 fold change from sex-matched wild-type, z-scored across rows. **E.** Number of genes within each cluster from D. Clusters with higher expression in females compared to males (XX-biased) highlighted in orange. **F.** UCSC browser view of a male and female shared germline DEG *D1Pas1* that is more highly expressed in female mutants (Average, n = 3). **G.** Left - Number of all female germline DEGs located on each chromosome over the total number of germline-enriched genes on that chromosome. Right - Percentage of germline DEGs that lie on each chromosome for each *Kdm5c* mutant. X chromosome highlighted in black. **H.** Sankey diagram classifying egg-biased (pink) and sperm-biased (blue) and unbiased (purple) mouse germline-enriched genes. **I.** Number of egg, sperm, or unbiased germline DEGs for male and female *Kdm5c* mutants. **J.** UCSC browser view of egg-biased (*Zp3*), sperm-biased (*Dkk1*), and unbiased (*Dazl*) germline genes dysregulated in both male and female *Kdm5c* mutants (Average of n = 3).

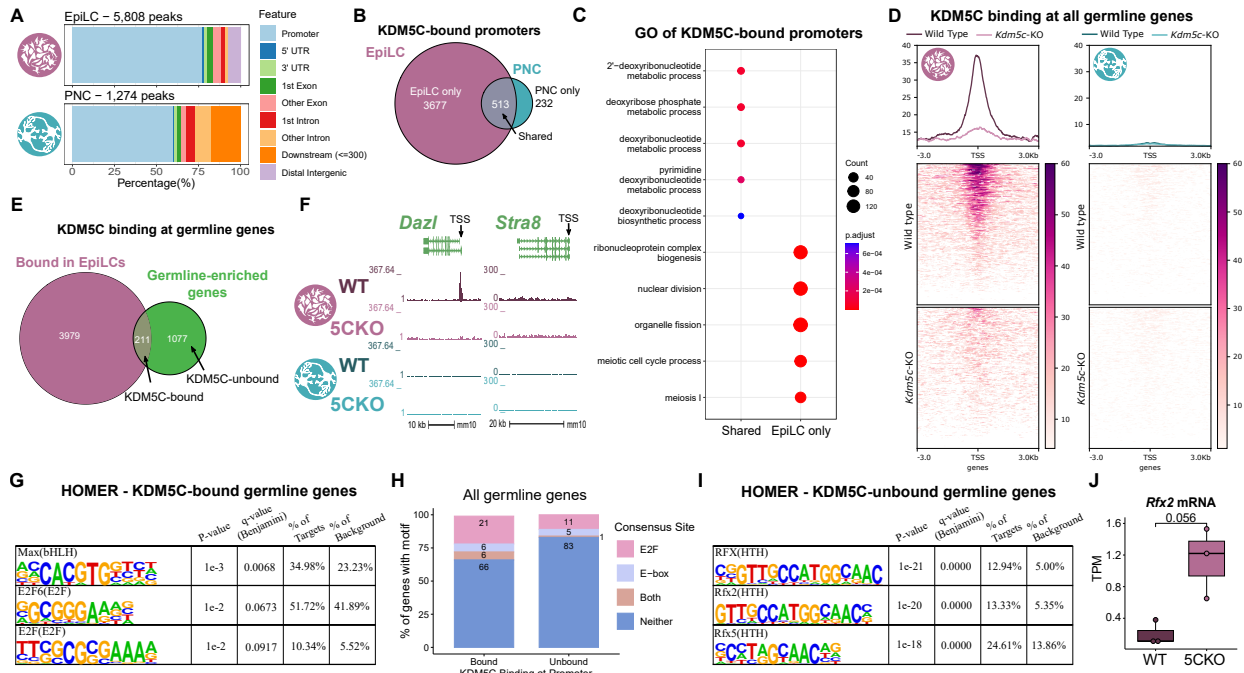


Figure 5: KDM5C binds to a subset of germline gene promoters during early embryogenesis. **A.** ChIPseeker localization of KDM5C peaks at different genomic regions in EpiLCs (top) and hippocampal and cortex primary neuron cultures (PNCs, bottom). **B.** Overlap of genes with KDM5C bound to their promoters ($TSS \pm 500$) in EpiLCs (purple) and PNCs (blue). **C.** Gene ontology (GO) comparison of genes with KDM5C bound to their promoter in EpiLCs and PNCs. Genes were classified as either bound in EpiLCs only (EpiLC only), unique to PNCs (PNC only, no significant ontologies) or bound in both PNCs and EpiLCs (Shared). **D.** Average KDM5C binding around the transcription start site (TSS) of all germline-enriched genes in EpiLCs (left) and PNCs (right). **E.** Eulerr overlap of germline-enriched genes (green) with significant KDM5C binding at their promoter in EpiLCs (purple). **F.** Example KDM5C ChIP-seq signal around the *Dazl* TSS but not *Stra8* in EpiLCs. **G.** HOMER motif analysis of all KDM5C-bound germline gene promoters, highlighting significant enrichment of MAX, E2F6, and E2F motifs. **H.** Number of all gene promoters bound or unbound by KDM5C with instances of the E2F or E-box consensus sequence. **I.** HOMER motif analysis of all KDM5C-unbound germline gene promoters, highlighting significant enrichment of RFX family transcription factor motifs. **J.** Expression of RNA-seq DEG *Rfx2* in wild-type and *Kdm5c*-KO EpiLCs. P-value of Welch's t-test, expression in transcripts per million (TPM).

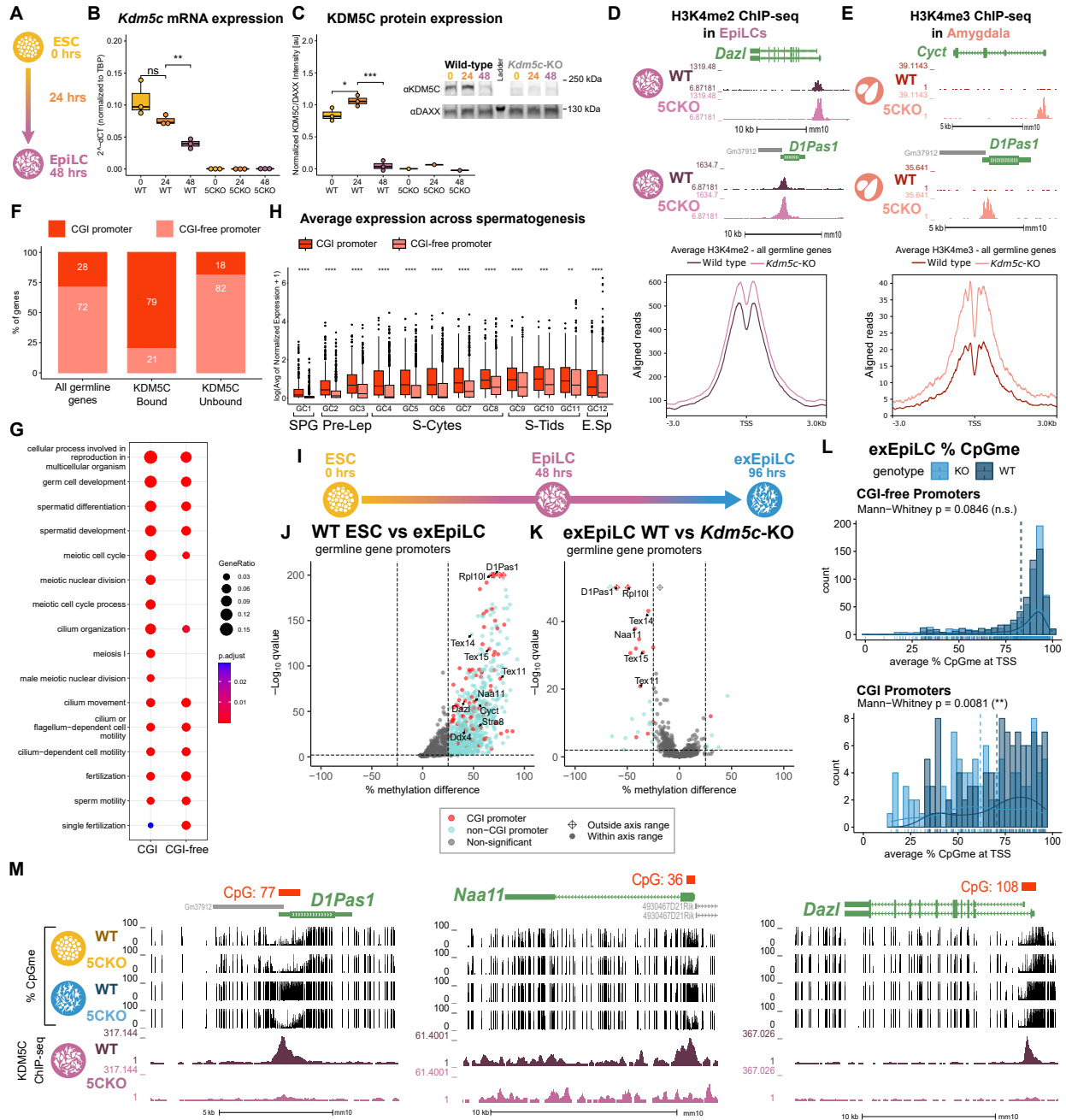


Figure 6: KDM5C promotes long-term silencing of germline genes via DNA methylation at CpG islands. **A.** Diagram of embryonic stem cell (ESC) to epiblast-like cell (EpiLC) differentiation and collection time points. **B.** Real time quantitative PCR (RT-qPCR) of *Kdm5c* mRNA expression in wild-type (WT) and *Kdm5c*-KO (5CKO) ESCs at 0, 24, and 48 hours of differentiation into EpiLCs. Expression calculated in comparison to TBP mRNA expression ($2^{-\Delta\Delta CT}$). * $p < 0.05$, ** $p < 0.01$, *** $p < 0.001$, Welch's t-test. **C.** KDM5C protein expression normalized to DAXX. Quantified intensity using ImageJ (artificial units - au). Right - representative lanes of Western blot for KDM5C and DAXX. * $p < 0.05$, ** $p < 0.01$, *** $p < 0.001$, Welch's t-test. **D.** Top - Representative UCSC browser view of histone 3 lysine 4 dimethylation (H3K4me2) ChIP-seq signal at two germline genes in wild-type and *Kdm5c*-KO EpiLCs. Bottom - Average H3K4me2 signal at the TSS of all germline-enriched genes in wild-type (dark purple) and *Kdm5c*-KO (light purple) EpiLCs. **E.** Top - Representative UCSC browser view of histone 3 lysine 4 trimethylation (H3K4me3) ChIP-seq signal at two germline genes in the wild-type (WT) and *Kdm5c*-KO (5CKO) adult amygdala. Bottom - Average H3K4me3 signal at the transcription start site (TSS) of all germline-enriched genes in wild-type (dark red) and *Kdm5c*-KO (light red) amygdala. **F.** Percentage of germline genes that harbor CpG islands (CGIs) in their promoters (CGI promoter, red), based on UCSC annotation. Left - percentage of all germline-enriched genes, middle - KDM5C-bound germline genes, and right - KDM5C-unbound germline genes. (Legend continued on next page.)

Figure 6: KDM5C promotes long-term silencing of germline genes via DNA methylation at CpG islands. (Legend continued.) **G.** enrichPlot gene ontology analysis of germline genes with (CGI-promoter) or without (CGI-free) CGIs in their promoter. **H.** Expression of germline genes with (CGI-promoter, red) or without (CGI-free, salmon) CGIs in their promoter across stages of spermatogenesis from Green et al 2018. SPG - spermatogonia, Pre-Lep - preleptotene spermatocytes, S-Cytes - meiotic spermatocytes, S-Tids - post-meiotic haploid round spermatids, E.Sp - elongating spermatids. Wilcoxon test, * $p < 0.05$, ** $p < 0.01$, *** $p < 0.001$, **** $p < 0.0001$. **I.** Diagram of ESC to extended EpiLC (exEpiLC) differentiation. **J.** Volcano plot of whole genome bisulfite sequencing (WGBS) comparing CpG methylation (CpGme) at germline gene promoters ($TSS \pm 500$) in wild-type (WT) ESCs versus exEpiLCs. Significantly differentially methylated promoters ($q < 0.01$, $|methylated difference| > 25\%$) with CGIs in red, CGI-free promoters in light blue **K.** Volcano plot of WGBS of wild-type (WT) versus *Kdm5c*-KO exEpiLCs for germline gene promoters. Promoters with CGIs in red, CGI-free promoters in light blue. **L.** Histogram of average percent CpGme at the promoter of germline genes with or without CGIs. Wild-type in navy and *Kdm5c*-KO (KO) in light blue. Dashed lines are average methylation for each genotype, p-values for Mann-Whitney U test. **M.** UCSC browser view of germline genes, showing UCSC annotated CGI with number of CpGs, representative CpGme in wild-type (WT) and *Kdm5c*-KO (5CKO) ESCs and exEpiLCs, and KDM5C ChIP-seq signal in EpiLCs.